

Spaceborne observations of the lidar ratio of marine aerosols

K. W. Dawson¹, N. Meskhidze¹, D. Josset^{2,#}, and S. Gassó³

¹Marine, Earth, and Atmospheric Science, North Carolina State University, Raleigh, NC, USA

²Science Systems and Applications, Inc/NASA Langley Research center

³GESTAR/Morgan State University, Goddard Space Flight Center, Greenbelt, Maryland

[#]Now at Naval Research Laboratory, Stennis Space Center,

Correspondence to: Nicholas Meskhidze (nmeskhidze@ncsu.edu)

Abstract

Retrievals of aerosol optical depth (AOD) from the Cloud-Aerosol Lidar with Orthogonal Polarization (CALIOP) satellite sensor require the assumption of the extinction-to-backscatter ratio, also known as the lidar ratio. This paper evaluates a new method to calculate the lidar ratio of marine aerosols using two independent sources: the AOD from the Synergized Optical Depth of Aerosols (SODA) and the integrated attenuated backscatter from CALIOP. With this method, the particulate lidar ratio can be derived for individual CALIOP retrievals in single aerosol layer, cloud-free columns over the ocean. Global analyses are carried out using CALIOP level 2, 5km marine aerosol layer products and the collocated SODA nighttime data from December 2007 to November 2010. The global mean lidar ratio for marine aerosols was found to be 26 sr, roughly 30% higher than the current value prescribed by the CALIOP standard retrieval algorithm. Data analysis also showed considerable spatiotemporal variability in the calculated lidar ratio over the remote oceans. The calculated aerosol lidar ratios are inversely related to the mean ocean surface wind speed: an increase in ocean surface wind speed (U_{10}) from 0 to >15 ms^{-1} reduces the mean lidar ratios for marine regions from 32 sr (for $0 < U_{10} < 4$ ms^{-1}) to 22 sr (for $U_{10} > 15$ ms^{-1}). Such changes in the lidar ratio are expected to have a corresponding effect on the marine AOD from CALIOP. The outcomes of this study are relevant for future improvements of the SODA and CALIOP operational product and could lead to more accurate retrievals of marine AOD.

1 Introduction

2
3 Marine aerosols are produced through primary emission of sea spray particles, and oxidation
4 of phytoplankton-produced dimethylsulfide and biogenic volatile organic carbon. Radiative
5 forcing by marine aerosol comprises a significant portion of the global energy budget. Studies
6 have shown that marine aerosol optical depth (AOD) is approximately 0.15 and likewise, the
7 contribution of marine aerosol to cloud condensation nuclei is about 60 cm^{-3} (Kaufman et al.,
8 2002; Lewis and Schwartz, 2004). Thus, marine aerosol is an important natural contributor to
9 global aerosol burden affecting both direct (i.e., extinction of solar radiation via scattering
10 and absorption) and indirect (i.e., cloud lifetime and frequency) radiative forcing of climate.
11 As marine aerosols contribute considerably to the preindustrial, natural background and
12 provide the base line on top of which anthropogenic forcing should be quantified, it is very
13 important to properly characterise marine aerosol burden and its spatiotemporal distribution.
14 The incomplete characterisation of background aerosols, of which marine particles are part
15 of, was shown to contribute large uncertainty in anthropogenic aerosol forcing calculations
16 and climate simulations (Ghan et al., 2001; Hoose et al., 2009; Wang and Penner, 2009;
17 Meskhidze et al., 2011; Westervelt et al., 2012; Carslaw et al., 2013).

18 Aerosols over the remote oceans come from natural continental (e.g., mineral dust and
19 biomass burning) and human-induced pollution (Andreae, 2007) in addition to marine
20 sources. Therefore, knowing horizontal and vertical distribution, as well as speciation of
21 aerosols becomes extremely important for the correct quantification of marine aerosol
22 radiative properties. The last decade has produced a large body of information regarding the
23 sources and composition of marine aerosol, resulting in a reassessment of the complex role
24 that marine aerosols play in climate and various geophysical phenomena. Passive satellite
25 instruments like the Sea-Viewing Wide Field-of-view Sensor (SeaWiFS), the MODerate
26 resolution Imaging Spectroradiometer (MODIS), and the Multi-angle Imaging
27 Spectroradiometer (MISR), as well as the ground-based AErosol RObotic NETwork
28 (AERONET) have contributed immensely to quantitative characteristics of marine aerosol in
29 terms of AOD (the column integrated aerosol extinction), size distribution information and
30 spectral optical properties. Although passive instruments have been useful for developing a
31 basic picture of marine aerosol distribution, they supply limited information on aerosol
32 speciation and very little data related to aerosol distribution in the vertical column. The
33 introduction of the Cloud-Aerosol Lidar with Orthogonal Polarization (CALIOP) onboard the
34 Cloud-Aerosol Lidar and Infrared Pathfinder Satellite Observations (CALIPSO) platform has

1 eliminated some of the assumptions made by the passive instruments and has provided a
2 more complete picture of the global aerosol distribution wanted by climate scientists.
3 However, CALIOP is an elastic backscatter lidar with no molecular filtering capability and
4 therefore requires the assumption of an extinction-to-backscatter ratio, also known as the
5 lidar ratio, to infer extinction from attenuated backscatter measurements. Depending on the
6 microphysical properties of the aerosol, the lidar ratio can have a wide range of values and
7 therefore a straightforward a-priori solution within some reasonable uncertainty range is
8 generally unobtainable without various assumptions or constraints. Theoretical calculations
9 for the lidar ratio can be performed, if the physicochemical properties and the size
10 distribution of the particles at the different heights in the vertical column are known;
11 however, the fulfillment of these requirements would make the lidar measurements
12 unnecessary (Ackermann, 1998). The typical solution to this problem is to assign a vertically
13 independent lidar ratio to aerosol retrievals that fit a specific aerosol model as outlined in
14 Omar et al. (2009).

15 To date, experimental techniques for directly measuring the lidar ratio include the use
16 of High Spectral Resolution Lidar (HSRL, Eloranta, 2005; Hair et al., 2008) and Raman
17 Lidar (RL, Ansmann et al., 1990). These instruments are capable of measuring aerosol
18 backscatter and extinction parameters independently and therefore do not require the lidar
19 ratio to be prescribed (e.g., Shipley et al., 1983; Grund and Eloranta, 1991; Piironen and
20 Eloranta, 1994; Müller et al., 2007; Amiridis et al., 2009; Tesche et al., 2009a,b; Burton et al.,
21 2012). On the other hand, Cattrall et al. (2005) use AERONET size distributions inverted
22 from sun photometer data (Holben et al., 1998) to calculate the lidar ratio and then compare
23 their indirect to literature reported direct measurements. They determined that their indirect
24 method (28 ± 5) compared well to the literature average of direct retrievals (29 ± 5) (see Tables
25 3 and 4 in Cattrall et al., 2005). Direct measurements do not suffer the same limitations as
26 indirect ones which require assumptions on size distribution and chemical composition or a
27 molecular extinction profile. The supplementary Table S1 summarises available retrieval
28 methods and values of some experimentally determined lidar ratios over marine regions.
29 Currently, most lidars do not yet have Raman or high spectral resolution capability and
30 CALIPSO is the only lidar that provides aerosol data at the vast spatiotemporal resolution
31 required for global climate model comparison.

32 Since the uncertainty in the lidar ratio can significantly affect the accuracy of the
33 aerosol extinction retrieval (see a detailed discussion below), lidar ratios have been
34 constrained by numerous approaches. However, marine aerosol size distribution, chemical

1 composition and refractive index can change significantly with ocean surface wind speed
2 (U_{10}), relative humidity (RH), temperature, salinity and chemical/biological composition of
3 surface sea water (de Leeuw et al., 2011; Lewis and Schwartz, 2004). For this reason, large
4 disagreement exists in the literature regarding the value of maritime aerosol lidar ratio (S_p ;
5 subscript “p” indicates particulate). For example, lidar measurements of (Ansmann et al.,
6 2001) over the North Atlantic showed $S_p = 24 \pm 5$ sr whereas measurements using a
7 nighttime lidar at a horizontal orientation off the northern coast of Queensland, Australia
8 showed maritime aerosol lidar ratios as high as $S_p = 39 \pm 5$ (Young et al., 1993). Using the
9 data from AERONET oceanic sites, Cattrall et al. (2005) derived a lidar ratio of 28 ± 5 sr, a
10 value that compared well with a literature averaged value of $S_p = 29 \pm 5$ sr (for $490 \leq$
11 $\lambda \leq 550$ nm) for maritime aerosols. Passive techniques have also been used to derive the
12 lidar ratio using an alternative definition of S_p as a function of single scattering albedo and
13 the scattering phase function near 180° (Bréon, 2013). Using the multi-directional
14 measurements of solar radiation from the polarization sensitive passive radiometer POLDER,
15 typical values for clean marine aerosol S_p were derived to be 25 sr at 532 nm (Bréon, 2013).
16 The lidar ratio of 20 ± 6 sr (at 532 nm) was selected for the CALIOP retrieval algorithm
17 based on parameters measured during the Shoreline Environmental Aerosol Study (SEAS)
18 experiment (Masonis et al., 2003; Omar et al., 2009). The SEAS measurements conducted on
19 the beach (downwind of an offshore reef) report a particulate lidar ratio $S_p = 25.4 \pm 3.5$ sr
20 at 532 nm based on the optical size measurements of marine aerosol, and an average modeled
21 value of $S_p = 20.3$ sr (Masonis et al., 2003). However, it was also shown that depending on
22 a particle size and wind speed regime S_p values can range from 10 to 90 sr (Masonis et al.,
23 2003; Sayer et al., 2012). Therefore, as size distribution (and chemical composition) of
24 marine aerosol may vary over the oceans, a constant lidar ratio used in CALIOP algorithms
25 may lead to erroneous retrievals of AOD.

26 In this study, we present a new method for deriving lidar ratios for individual
27 CALIOP retrievals of single aerosol layer columns over the ocean. We have used the
28 Synergized Optical Depth of Aerosols (SODA) product (described in section 2.2) to estimate
29 S_p for a strictly defined subset of CALIPSO data. The S_p values are calculated as a
30 correction to achieve the best agreement between SODA and CALIPSO marine aerosol AOD
31 values. Using CALIPSO level 2 aerosol layer data for years 2007 to 2010, we have created a
32 3-year averaged climatology of clean marine aerosol lidar ratio over the globe. Analyses were
33 also carried out to assess dependence of S_p values on wind speed and estimate possible error

1 sources in our calculations.

2 **2 Instrumentation and Methods**

3 **2.1 CALIPSO satellite**

4 The CALIPSO mission (Winker et al., 2009), launched on April 28, 2006, has been able to
5 provide the scientific community with vertically resolved measurements of both aerosol and
6 cloud optical properties like depolarization ratio (a measure of particle sphericity), AOD, and
7 ice/water phase since June 2006. The CALIPSO payload includes a high-powered digital
8 camera, an infrared radiometer, and a two-wavelength (532 and 1064 nm), near nadir,
9 polarization sensitive, elastic backscatter lidar, CALIOP.

10 The level 1 data algorithms are responsible for the geolocation and range
11 determination of the satellite and produce profiles of attenuated backscatter coefficients. Data
12 in this work were obtained from the 5 km, level 2 operational products version 3.01. Level 2
13 products have undergone various processing algorithms from the Selective Iterated Boundary
14 Locator (SIBYL), the Scene Classification Algorithm (SCA), and the Hybrid Extinction
15 Retrieval Algorithm (HERA) (Vaughan et al., 2004; 2009). First, SIBYL identifies layers,
16 then the SCA identifies the type of feature (i.e., aerosol or cloud) and the subtype (i.e.,
17 aerosol type, ice/water phase), and finally, the HERA generates extinction profiles for the
18 feature. The theoretical basis of the algorithm can be found online at
19 www-calipso.larc.nasa.gov/resources/project_documentation.php.

20 The CALIPSO 5 km aerosol layer data includes many operational products of which
21 only a few are used in this study. Among them are, the integrated attenuated backscatter
22 and its uncertainty at 532 nm, the layer features such as number found in the column and their
23 top and bottom altitudes and the feature classification flags.

24 **2.2 Synergized Optical Depth of Aerosols (SODA)**

25 CloudSat was launched in 2006 with CALIPSO and was positioned in sun-synchronous orbit
26 as part of the A-Train satellite constellation. CloudSat and CALIPSO have paved the way for
27 new multi-sensor data products like SODA to be developed. The main instrument on
28 CloudSat is the Cloud Profiling Radar (CPR), a nearly nadir looking (0.16°) 94-GHz (≈ 3
29 mm; W-band) radar. The CPR, like CALIOP, can retrieve information on hydrometeor
30 microphysical properties at different heights in a vertical column. The CPR signal is mostly

1 attenuated by water vapor; however, for cloud free regions over the ocean, the CPR data can
 2 be used to retrieve AOD. A method developed by Josset et al. (2008) and later expanded by
 3 Josset et al. (2010a) uses a combination of CALIOP and CPR measurements of the ocean
 4 surface reflectance to derive AOD. The design of SODA utilises the ratio of the radar-to-lidar
 5 ocean surface scattering cross section to infer column optical depth for non-cloudy
 6 atmospheric columns. Since the radar signal attenuates mostly due to water vapor and the
 7 lidar signal weakens mostly due to aerosols, after the radar signal is corrected for attenuation
 8 by water vapor and oxygen, the change in the radar-to-lidar signal ratio is directly related to
 9 aerosol abundance (Josset et al., 2008; 2010a). Therefore, by using observations from two
 10 different sensors, SODA can eliminate uncertainties induced by the CALIOP aerosol
 11 extinction algorithm over oceans. SODA AODs have been shown to be in very good
 12 agreement with MODIS AOD retrievals (Josset et al., 2008). A more detailed description of
 13 the SODA technique and its application is given in Josset et al. (2008; 2010a; 2010b; 2011;
 14 and 2012). The SODA products that are used in this study include the quality assurance
 15 measure "qa_flag_aerosol" and the 532 nm AOD.

16 2.3 Lidar ratio definition

17 One of the biggest advantages of the SODA product is that it removes the dependence of the
 18 prescribed lidar ratio while still utilizing the active sensors to retrieve an AOD, thereby
 19 providing a means for independent evaluation of the lidar ratio. In the current study we use
 20 Eq. 4 from Josset et al. (2011) to estimate lidar ratio from CloudSat/CALIOP measurements
 21 of AOD values. Following Fernald et al. (1972), the particulate two-way transmittance at
 22 height Z can be written as:

$$T^2(Z) = e^{-2S_p \int_0^Z \beta_p(z) dz} \quad (1)$$

23 where the lidar ratio at height Z can be defined as the ratio of the particulate extinction to
 24 backscatter $\left(S_p = \frac{\sigma_p(Z)}{\beta_p(Z)}\right)$. Differentiating Eq. 1 with respect to vertical coordinate (z) gives
 25 the particulate backscatter at height Z :

$$\beta_p(Z) = -\frac{1}{2S_p T^2(Z)} \frac{dT^2(Z)}{dZ} \quad (2)$$

26 Since atmospheric constituents (molecules and different particle types) can interact with the
 27 lidar beam at different heights, the lidar ratio using remotely sensed data cannot be uniquely
 28 defined for a given atmospheric column. However, the lidar ratio is a particle intensive
 29 property (i.e., dependent on particle type and not on the amount). So, if we assume that there

1 is only a single type of aerosol and it is homogeneously distributed throughout the
 2 atmospheric column and that molecular scattering is sufficiently removed by the CALIOP
 3 level 2 algorithms, then the column lidar ratio ($\overline{S_p}$) can be expressed as the ratio of the
 4 particulate column integrated extinction ($\overline{\tau_p} = \text{AOD}$) to the attenuated backscatter ($\overline{\Gamma_p}$). Based
 5 on these assumptions, integration of Eq. 2 with respect to vertical coordinate gives the
 6 particulate lidar ratio as:

$$\overline{S_p} = \frac{\int_{T_p^2(0)}^{T_p^2(z)} dT^2(z)}{\int_0^z \beta_p(z) T_p^2(z) dz} \quad (3)$$

7 If we first substitute in Eq. 3 the definition for two-way transmittance as $T_p^2 = e^{-2\overline{\tau_p}}$, then
 8 substitute the total particulate attenuated backscatter signal retrieved by the lidar as
 9 $\overline{\Gamma_p} = \int_0^z \beta_p(z) T_p^2(z) dz$ and finally consider that $T_p^2(0) = 1$, the equation for a columnar
 10 particulate lidar ratio is:

$$\overline{S_p} = \frac{1 - e^{-2\overline{\tau_p}}}{2\overline{\Gamma_p}} \quad (4)$$

11 Equation 4 allows us to calculate marine aerosol lidar ratio from two independent sources: the
 12 AOD (i.e., $\overline{\tau_p}$) from SODA and the integrated attenuated backscatter ($\overline{\Gamma_p}$) from CALIOP. It
 13 should be noted that CALIOP estimation of $\overline{\Gamma_p}$ is difficult for layers that are not bounded by
 14 clear air (Vaughan et al., 2004) and therefore require carefully designed data screening
 15 algorithms. In section 4 we carry out an error analysis to verify that uncertainties in $\overline{\Gamma_p}$ have
 16 a minimal effect on the retrieved lidar ratio.

17 2.4 Data selection method

18 As different aerosol sub-types have different lidar ratios, application of Eq. 4 to episodes
 19 when aerosols other than marine aerosols are present in the atmospheric column may lead to
 20 erroneous results for the calculated $\overline{S_p}$. We developed a strict scene selection algorithm to
 21 minimise the contamination of AOD and therefore $\overline{S_p}$ by aerosol types other than marine
 22 (e.g., anthropogenic pollution, biomass burning, and dust). The algorithm first uses the
 23 feature classification flags in the CALIOP aerosol layer product. We start with clean marine
 24 aerosol that is identified based on surface type (as determined by the location of the satellite)
 25 and then retain only the data with total integrated attenuated backscatter $\gamma' < 0.01 \text{ km}^{-1} \text{sr}^{-1}$
 26 and volume depolarization ratio $\delta' < 0.05$ (Omar et al., 2009). As multiple types of aerosols

1 can be found within retrieved vertical profiles (e.g., dust above marine aerosols), aerosol
 2 feature types that have been identified as marine in a given atmospheric column are not
 3 enough to carry out the analysis. Therefore, when determining the lidar ratio of marine
 4 aerosol using Eq. 4, the algorithm only retains the data in which clean marine is the only type
 5 of aerosol present in the entire cloud-free atmospheric column. To further reduce the
 6 uncertainty, we constrain the analysis to single layer profiles below 2 km and remove profiles
 7 in which marine aerosol layers are vertically stacked within an atmospheric column.
 8 Therefore, the vertically integrated particulate attenuated backscatter $\overline{\Gamma}_p$ is replaced by Γ_p .
 9 Similarly, the column lidar ratio \overline{S}_p is reduced to S_p in the remainder of the text. Note also
 10 that all quantities discussed are particulate quantities and therefore, molecular scattering is
 11 removed using gridded molecular and ozone number density profile data from the Goddard
 12 Earth Observing System Model, version 5 (GEOS-5) analysis product available from the
 13 NASA Global Modeling and Assimilation Office (GMAO) (Winker et al., 2009).
 14 Operationally, particulate scattering is determined to be where the ratio of the CALIOP 532
 15 nm scattering profile normalised by the GEOS-5 molecular scattering profile is greater than
 16 one ($\frac{\beta'_{532}}{\beta_m} > 1$). Errors associated with $\overline{\Gamma}_p$ are discussed in Sec. 4.

17 All data is for nighttime and is binned into $2^\circ \times 5^\circ$ latitude and longitude, respectively,
 18 grid cells. Collocated wind speed is taken from the Advanced Microwave Scanning
 19 Radiometer - Earth (AMSR-E) observing system. To identify distinct features associated with
 20 the variability in marine aerosol lidar ratio over different parts of the oceans, the selected data
 21 is examined in relation with other variables such as season, spatial location and wind speed.

22 Some additional measures were taken to target layers with a high signal-to-noise ratio
 23 and grid cells with a significant number of observations. These measures included (i)
 24 ensuring the relative error in Γ_p due to random noise in molecular backscatter was $< 50\%$,
 25 (ii) the collocated SODA 5 km layer was composed of at least 70% shot-to-shot data and (iii)
 26 the total number of retrievals per $2^\circ \times 5^\circ$ grid cell ranked above the first quartile of the grid
 27 cell frequency distribution. Such strict quality controls considerably increase the reliability of
 28 the analysis despite reducing the total number of data points. It should be noted that a large
 29 number (over 260,000) of data points remained for robust statistics after all the quality
 30 control and quality assurance tests. A caveat, despite such rigorous quality control criteria,
 31 remains when interpreting data near coastlines as the CALIOP scene classification algorithm
 32 may mistakenly identify mixtures of continental pollution and marine as clean marine aerosol
 33 (Burton et al., 2013; Oo and Holz, 2011; Schuster et al., 2012) causing an overestimation in

1 the lidar ratio inferred from Eq. 4. Further discussion of error analysis is given in Sec. 4.

2

3 **3 Results**

4 **3.1 Global distribution of retrieved AOD and lidar ratio**

5 Active detectors like CALIOP require knowledge of the lidar ratio for retrieval of
6 aerosol optical properties. Incorrect estimates of the S_p values for a given aerosol type can
7 lead to significant errors in the retrievals of particulate extinction and AOD. Past studies
8 using collocated CALIOP and MODIS retrievals have shown that, over the marine regions,
9 CALIOP underestimates the AOD values relative to MODIS (Oo and Holz, 2011). As
10 MODIS data over the ocean has been extensively evaluated with numerous field campaigns
11 (e.g., Levy et al., 2005), it was suggested that the primary source of discrepancy between the
12 two sensors was the low value of the marine aerosol lidar ratio used by CALIOP (Oo and
13 Holz, 2011). Figure 1 shows seasonally averaged maps of CALIPSO and SODA marine
14 aerosol median optical depth at 532 nm and the differences between SODA and CALIOP
15 retrieved AODs. White regions on Fig. 1 represent grid cells that were rejected by the data
16 selection algorithm and have been removed from the subsequent data analysis. Inspection of
17 Fig. 1 reveals considerable spatial and temporal variations in marine aerosol AOD. Although
18 the largest values of AOD seem to occur over regions with higher surface wind speed (i.e.,
19 the northern and southern oceans), elevated AOD values can also be seen over the regions
20 downwind from dust and/or pollution sources such as the mid-latitude North Atlantic Ocean
21 and the Bay of Bengal and over the major oceanic gyres. The region around the Indian
22 subcontinent and over the Bay of Bengal is believed to be just a retrieval artifact. Large
23 disagreements between SODA and CALIOP reported AODs for these regions suggest that
24 some dust/pollution aerosols might have been misclassified by CALIOP as marine aerosol.
25 Higher S_p values for dust and pollution compared to marine aerosol would produce a higher
26 AOD retrieval in SODA compared to CALIOP. Elevated AOD values over the oceanic
27 regions with lower surface wind speed, on the other hand, could point to changes in marine
28 aerosol size distribution to smaller sizes. Sub-micron sea salt aerosols (with particle diameter,
29 $D_p < 1 \mu\text{m}$) are believed to have larger lidar ratios than super-micron ones (e.g., Masonis et
30 al., 2003; Oo and Holz, 2011). In general, Fig. 1 shows positive differences between SODA
31 and CALIOP retrieved seasonal median AOD values. Recalling that CALIOP retrieved
32 extinction is the product of the prescribed lidar ratio and the measured column integrated

1 particulate backscatter, positive differences between SODA and CALIOP median AODs at
2 532 nm over most of the oceans suggest underestimation of the marine aerosol lidar ratio
3 prescribed in the CALIOP clean marine aerosol model. Figure 2 shows that over most of the
4 ocean surfaces, the calculated lidar ratio is higher than the default ($S_p = 20$ sr) used in the
5 CALIOP clean marine aerosol model. Global means and standard deviations for AOD and
6 lidar ratio are given in Table 1. CALIOP retrievals in this study cannot be directly compared
7 to MODIS since we only use nighttime data. Nevertheless, SODA retrievals of AOD have
8 been shown to agree well with MODIS (Josset et al., 2008), HSRL (Fig. 6; Josset et al., 2011)
9 and Maritime Aerosol Network (Smirnov et al., 2011; supplementary information Fig. S3)
10 observations suggesting that the corrected lidar ratios will bring CALIOP retrievals close to
11 MODIS data. Figure 2 also reveals that the value of the lidar ratio calculated using Eq. 4
12 changes considerably over different parts of the remote oceans, pointing to the variability in
13 marine aerosol optical properties. It has long been known that meteorological and/or
14 environmental factors and ocean chemical/biological composition influence marine aerosol
15 production, entrainment, transport, and removal processes (Lewis and Schwartz, 2004) that
16 can ultimately affect marine aerosol S_p . Moreover, due to atmospheric transport of marine
17 aerosol, satellite retrieved AOD values may also be related to the upwind processes. Despite
18 the complexity of the mechanisms controlling marine aerosol mass concentration over the
19 oceans, surface wind speed has always been considered as the major parameter governing the
20 production, chemical composition, and life cycle of marine aerosol (Lewis and Schwartz,
21 2004). Therefore, in the next section we will investigate the effect of wind speed on
22 calculated temporal variability of marine aerosol lidar ratio.

23 3.2 Wind speed dependence

24 Numerous investigators have examined the effect of sea surface wind speed and sea state on
25 marine aerosol optical properties (e.g., Smirnov et al., 2003; Sayer et al., 2012). There are
26 two mechanisms for primary marine aerosol production: bursting of bubbles at the water
27 surface, and mechanical tearing of water drops (spume) from wave crests (for surface wind
28 speeds $U_{10} > 9$ ms⁻¹, Anguelova et al., 1999). Ocean bubbles are generated by the
29 entrainment of air due to wave action. As bubbles rise due to their buoyancy, they burst at the
30 surface producing marine aerosol (Blanchard and Woodcock, 1957). In this study we have
31 selected seven different wind speed regimes (see Table 2). The lowest wind speed regime,
32 $0 < U_{10} \leq 4$ ms⁻¹, was chosen to represent aerosols not generated via wind driven processes

1 over the ocean. In general, ocean waves break at wind speed values above $\sim 4 \text{ ms}^{-1}$ (initiating
2 the white cap formation and bursting of the entrained bubbles) (Lewis and Schwartz, 2004).
3 Therefore, it has been suggested that below this threshold value, there should be a weak
4 relationship between marine aerosol optical properties and the surface wind speed
5 (Kiliyanpilakkil and Meskhidze, 2011; Lehahn et al., 2010). Moreover, for such a low wind
6 speed regime, most of the aerosols classified as clean marine by CALIOP are either produced
7 outside the swath and then blown into the satellite field of view, or like in cases near
8 coastlines, mistakenly identified as marine aerosol. The highest wind speed regime, with U_{10}
9 $> 15 \text{ ms}^{-1}$, typically contributes a small fraction of CALIOP retrievals (Kiliyanpilakkil and
10 Meskhidze, 2011) and is largely concentrated over the southern ocean and in the northern
11 Atlantic where the highest wind speeds are observed (Bentamy et al., 2003). Although
12 CALIOP retrieval counts for marine aerosol in each $2^\circ \times 5^\circ$ grid cell are also influenced by
13 the presence of clouds, Fig. S1 shows the global distributions of CALIOP retrieval
14 frequencies for different wind speed regimes. Figure 3 shows the scatterplots for SODA and
15 CALIOP retrieved AOD values for the wind speed regimes of Table 2. As expected, Fig. 3
16 shows that increases in wind speed are typically associated with higher values of marine
17 aerosol optical depth (note the center of the scatter distribution shifts to higher AODs for
18 larger wind speed values). However, as the majority of the SODA AODs exist above the 1:1
19 line, this figure also indicates the underestimation of CALIOP retrieved marine aerosol
20 optical depth values. When averaged over the entire globe, CALIOP retrieved clean marine
21 AOD is roughly 32% lower compared to SODA. According to Fig. 3 the largest discrepancies
22 between SODA and CALIOP retrievals are observed at lower wind speed values. One simple
23 explanation for this is a greater chance for CALIOP misclassification over the oceanic
24 regions where long-ranged continental aerosols can contribute a larger fraction of the MBL
25 particles (e.g., Blot et al., 2013). Terrestrial particles (e.g., mineral dust, anthropogenic
26 pollution) are typically characterised by the larger lidar ratio values, leading to an
27 underestimation of the CALIOP retrieved AODs. However, measurements also show that
28 changes in surface wind speed values can cause a considerable shift in the marine aerosol size
29 distribution. For optically active marine aerosols, the residence time decreases considerably
30 with increasing size. Thus the aerosol population is increasingly controlled by the smaller end
31 of the particle size spectrum as wind speeds decrease over the ocean (Hoffman and Duce,
32 1974). Conversely, as wind speed increases, fine mode aerosol volume size distribution
33 changes slightly (with mixed trends), while the coarse mode volume size distribution exhibits
34 a large and positive response to the increase in wind speed (Lewis and Schwartz, 2004;

1 Smirnov et al., 2003). Such variability in marine aerosol volume size distribution is expected
2 to have an effect on the aerosol lidar ratio. As sub-micron marine aerosols are characterised
3 with much larger lidar ratios than super-micron ones (e.g., Masonis et al., 2003; Oo and Holz,
4 2011), shifting marine aerosol size distribution spectra to smaller particles will cause an
5 increase in total aerosol lidar ratio. Therefore, for clean MAs, AODs and lidar ratios are
6 expected to have opposite dependences on wind speed: high wind speed regions are
7 characteristic of high AODs and low lidar ratios while lower wind speeds favor higher lidar
8 ratios and lower AODs (Smirnov et al. 2003; Sayer et al., 2012).

9 Figure 4 shows that on average, the calculated aerosol lidar ratio is weakly related to
10 the surface wind speed. According to this figure, aerosols retrieved in the wind speed regime
11 $0 < U_{10} \leq 4 \text{ ms}^{-1}$ depict the largest variability in the lidar ratio as indicated by the spread of
12 the distribution. As discussed above, aerosols in this regime likely include both marine
13 aerosols particles produced upwind and advected into the satellite field of view (with $S_p \sim$
14 20 to 30 sr), as well as dust/pollution particles (with $S_p \sim 40$ to 70 sr, Omar et al., 2009) that
15 may have been misclassified by CALIOP as marine aerosol. As shown in Table 2, marine
16 aerosol lidar ratio distribution in this regime is characterised by the largest standard deviation
17 ($\sigma = 17.4 \text{ sr}$) indicating that for the lowest wind speed values, a wide range of marine
18 aerosol sizes can be present over the ocean. Since for the wind speed values less than 4 m s^{-1} ,
19 the primary marine aerosol production is minimal, such large spread could also indicate that
20 under low wind conditions there is greater probability for natural continental and
21 human-induced pollution aerosols be miss-classified by CALIOP as clean marine.

22 For the higher wind speed values ($4 < U_{10} \leq 15 \text{ ms}^{-1}$) lidar ratio generally decreases
23 with the increase in the wind speed and approaches the lidar ratios prescribed by CALIOP
24 retrieval algorithms (i.e., 20 sr) at the highest wind speed regime. According to Table 2 and
25 Fig. S1, the most common wind values in CALIOP marine aerosol retrievals over the ocean
26 are in the $8 < U_{10} \leq 10 \text{ ms}^{-1}$ regime (26% of all available data) followed by the $6 < U_{10} \leq$
27 8 ms^{-1} regime (23% of all available data). For the higher wind speed regimes ($U_{10} \gtrsim$
28 6 ms^{-1}), surface winds play a decisive role in the determination of the lidar ratio (indicated
29 by the narrow standard deviation, see Table 2). This is an important result as the distributions
30 shown on Fig. 4 may help in providing additional criteria for clean marine lidar ratio
31 selection, yielding improved retrieval of marine aerosol AOD from CALIOP.

32 Analysis of data indicates that a mean lidar ratio of 26 sr is the most probable value
33 that occurs for the majority of CALIOP retrievals over the oceans. This value compares well

1 with those reported in the literature. Müller et al. (2007) found a marine aerosol lidar ratio of
2 23 ± 3 and 23 ± 5 sr using RL and Burton et al. (2012; 2013) reported a range from 15-27 sr
3 using HSRL. Bréon (2013) used a different space-based retrieval and saw S_p for marine
4 aerosol is typically on the order of 25 sr. Table S1 reports some additional values of marine
5 aerosol S_p measured by other techniques. This new lidar ratio reduces discrepancy between
6 CALIOP-prescribed and SODA-derived lidar ratios from about 30% to 4%.

7 Previous studies reported small decrease in marine aerosol lidar ratio with the increase
8 in wind speed (Sayer et al., 2012). In general, wind speed alone is expected to be a poor
9 predictor of marine aerosol lidar ratio, as aerosol volume size distribution and optical
10 properties are likely to be influenced by a number of other parameters including relative
11 humidity and marine boundary layer depth. Nevertheless, as wind speed dependence of
12 marine aerosol S_p is of considerable interest for the remote sensing community we have
13 developed a parameterization of the lidar ratio with wind speed and include as a part of the
14 supplementary information (see Fig. S2). The parameterization is based on a full range of
15 wind speed values from 0 - 25 ms^{-1} , but given the low number of retrievals at very low (< 4
16 ms^{-1}) and very high ($> 15 \text{ms}^{-1}$) wind speeds, along with the large range of lidar ratios
17 retrieved at low wind speeds (roughly ± 17 sr), we recognise the need for further constraints
18 in these regions. Overall, given the number of retrievals and confidence bounds, we believe
19 our parameterization can be a useful tool for predicting marine aerosol S_p ($\lambda = 532 \text{nm}$)
20 at wind speeds between 8 and 15 ms^{-1} with an error of ± 2 sr. The main caveat to this
21 parameterization is the uncertainty of the spread at low wind speeds. Errors increase
22 exponentially approaching the lowest optical depths and could be the reason for the large
23 spread in the lidar ratio. Untangling systematic error from real physical effects is difficult in
24 the low (0-4 m/s) wind speed regime and highlights the need for more accurate measurements
25 for calm wind/low AOD conditions.

26 **4 Uncertainties, errors and sensitivity**

27 The method used to derive the lidar ratio in this study depends on two parameters: the
28 CALIOP integrated attenuated particulate backscatter (Γ_p) and the SODA aerosol optical
29 depth (τ_p). Uncertainties in both Γ_p and τ_p retrievals are expected to propagate through
30 the calculations of the particulate lidar ratio. Josset et al. (2008; 2010a) investigate the
31 domain of validity for τ_p through an extensive calibration procedure. They find that for
32 retrievals at wind speeds between 3 and 10 ms^{-1} the SODA product is in very good agreement

1 ($R > 0.89$) with MODIS AOD with calibration errors less than 15%. Calibration errors in
 2 τ_p are expected to be even lower for nighttime retrievals used in this study (Josset et al.
 3 2008). On the other hand, average uncertainty for CALIOP Γ_p retrievals has not been
 4 examined previously and will be determined below.

5 Since ocean is the source of marine aerosol, clean marine aerosol layers typically
 6 extend to the ocean surface. This makes it more difficult to determine molecular and
 7 particulate backscatter components of the signal separately using satellite measurements
 8 alone. To assess the uncertainty in lidar ratio introduced for the surface connected layers (i.e.,
 9 layers whose bottom bound is defined as the ocean surface), here we estimate the error in
 10 CALIOP retrieved Γ_p values. The total attenuated backscatter signal measured by the lidar
 11 consists of molecular and particulate components:

$$\beta_{att} = (\beta_p + \beta_m) e^{-2\tau_p} \cdot e^{-2\tau_m} \quad (5)$$

12 with subscripts m and p representing molecular and particulate quantities, respectively. From
 13 the definition of Γ_p it follows that:

$$\Gamma_p = \int_0^Z \beta_p(z) e^{-2\tau_p} dz \quad (6)$$

14 where the integration is from the surface to the top of the layer. β_p is the particulate
 15 backscatter and $e^{-2\tau_p}$ accounts for the attenuation of the lidar signal by the particles.
 16 Substituting Eq. 5 into Eq. 6 gives:

$$\Gamma_p = \int_0^Z (\beta_{att} e^{2\tau_m} - \beta_m(z) e^{-2\tau_p}) dz \quad (7)$$

17 The molecular component of the signal in Eq. 7 can be derived from the GMAO modeled
 18 temperature and pressure profiles (Bloom et al., 2005). However, to solve this equation and
 19 determine the particulate attenuated backscatter value, particulate column integrated
 20 extinction is required. To get τ_p the CALIOP algorithm is using a prescribed value of the
 21 lidar ratio, making Eq. 4 circularly dependent on the lidar ratio. The error in CALIOP
 22 retrieved Γ_p associated with the prescribed lidar ratio can be estimated by substituting the
 23 τ_p value from SODA. If the error is large, that would imply that the uncertainty in CALIOP
 24 prescribed lidar ratio would introduce sizable corrections to Γ_p , making Eq. 4 unsuitable for
 25 the estimation of marine aerosol lidar ratio.

26 The relative error in Γ_p can be defined as:

$$Error = \frac{\Gamma_{p,S} - \Gamma_{p,C}}{\Gamma_{p,C}} = \frac{(e^{-2\tau_{p,C}} - e^{-2\tau_{p,S}}) \cdot \int_0^Z \beta_m(z) dz}{\Gamma_{p,C}} \quad (8)$$

1 where $\Gamma_{p,S}$ and $\Gamma_{p,C}$ are columnar integrated attenuated backscatter values for SODA and
 2 CALIOP, respectively. From the theoretical basis documents for CALIOP level 1 algorithms,
 3 the molecular backscatter is estimated as $\beta_m = \frac{C_s T(z)}{S_m P(z)}$ where height dependent $T(z)$ and
 4 $P(z)$ profiles from the surface (1000 hPa) to top-of-atmosphere (0.1 hPa) pressure levels were
 5 obtained from the GMAO Modern-Era Retrospective analysis for Research and Applications
 6 dataset. The molecular lidar ratio, S_m is defined as $8\pi/3$ and C_s is a constant equal to
 7 3.742×10^{-6} K/hPa/m (Hostetler et al., 2005). When considering all of the parameters, our
 8 analysis shows that the average error in Γ_p is approximately 1.5%. Compared to the
 9 systematic uncertainty in the SODA product ($< 15\%$), the uncertainty in Γ_p is much lower
 10 indicating that, on average, errors in Γ_p do not dominate S_p retrievals. Since an average
 11 discrepancy between CALIOP-prescribed and SODA-derived lidar ratios ($\sim 30\%$) is more
 12 than an order of magnitude higher than uncertainty in Γ_p , we conclude that the uncertainty in
 13 the CALIOP column integrated backscatter has a minor effect on the Eq. 4 calculated lidar
 14 ratio.

15 Furthermore, because in our study we use feature integrated products for a single
 16 aerosol layer, it is also important to evaluate the relationship between Γ_p and aerosol layer
 17 thickness (ΔZ). Figure 5 shows the normalised column attenuated particulate backscatter Γ_p
 18 as a function of layer depth. For uniformly distributed aerosols throughout the column, Γ_p is
 19 likely to be proportional to ΔZ . The spread of $\Gamma_p/\Delta Z$ ratio is indicative of different amounts
 20 of marine aerosol present in the column. Two limits of very high and very low ΔZ values are
 21 of particular interest. For example, strong reduction of the $\Gamma_p/\Delta Z$ ratio at the higher ΔZ
 22 values would indicate that the lidar signal is strongly attenuated throughout the layer reaching
 23 a sensitivity limit. On the other hand, considerable increase of the ratio for the thin layers
 24 may indicate contamination of the backscattered signal by the surface reflectance. According
 25 to Fig. 5 for the vast majority of the data, signal attenuation and surface reflectance do not
 26 seem to be major issues for the surface connected layers, suggesting that the quality control
 27 algorithm described in Sec. 2.4 was sufficient to remove the majority of erroneous measures
 28 of Γ_p .

29 To further assess the reliability of SODA marine aerosol product we also compared
 30 collocated HSRL and SODA AOD data. Figure 6a shows results from three CALIPSO (and
 31 therefore SODA) underflights validated against HSRL. According to Fig. 6a for AODs < 0.3
 32 (comprising the majority of marine aerosol retrievals), SODA compares reasonably well to

1 HSRL ($R^2 = 0.82$, $RMSE = 0.04$; similar to the MAN comparison with $RMSE = 0.03$ in
2 supplementary Fig. S3). Additionally, Fig. 6b illustrates that the relative uncertainty in the
3 SODA retrieved S_p is typically below 50% for AODs > 0.05 . In our study, the bulk of AODs
4 measured by SODA (98%) exceed this value under the quality control criteria discussed in
5 Sec. 2.4. Errors were estimated based on Eq. 15 in Josset et al. (2012) and for AODs > 0.05 ,
6 we expect lidar ratio retrieval uncertainties below 50%.

7 **5 Conclusions**

8 A new method showing that it is possible to infer lidar ratios of marine aerosol over the ocean
9 using two independent sources: the AOD from Synergized Optical Depth of Aerosols
10 (SODA) and the integrated attenuated backscatter from Cloud-Aerosol Lidar with Orthogonal
11 Polarization (CALIOP) has here been applied. The proposed equation calculates particulate
12 lidar ratio for individual CALIOP retrievals of single aerosol layer columns as a correction to
13 achieve the best agreement between SODA and CALIOP retrievals. The new method allows
14 calculating marine aerosol lidar ratio and assessing its spatiotemporal variability and
15 dependence on ocean surface wind speed. Analyses were carried out using CALIOP level 2,
16 5km aerosol layer and collocated SODA nighttime data from December 2007 to November
17 2010. During the data analysis over 260,000 data points passed various quality-control and
18 quality-assurance tests to reduce errors associated with the clean marine aerosol retrievals.
19 The calculated lidar ratios have been analysed over the global ocean covering a wide range of
20 wind speed and AOD conditions. Data analysis shows that over most of the ocean surfaces,
21 the calculated lidar ratio is higher than the default lidar ratio of 20 sr used in the CALIOP
22 clean marine aerosol model. The calculated aerosol lidar ratios are inversely related to the
23 surface wind speed. Increases in mean surface ocean wind speeds from 0 to $>15 \text{ ms}^{-1}$ reduces
24 the mean lidar ratio for marine aerosol from ~ 32 sr to ~ 22 sr. Such reduction was explained
25 by the shift in aerosol volume size distribution with the wind speed; however, it was also
26 emphasised that future studies should explore the role of meteorological and/or
27 environmental factors and ocean chemical/biological composition for marine aerosol
28 intensive properties. Our data analysis showed that changes in wind speed also affect the
29 probability density function for marine aerosol lidar ratio distribution. The largest standard
30 deviation calculated for the lowest wind speed regime suggested that under low wind
31 conditions, a wide range of marine aerosol sizes can be present over the ocean and there is
32 greater probability for natural-continental and human-induced pollution aerosols to be

1 classified by CALIOP as clean marine. We would like to mention that the role of organic
2 aerosol at low wind speeds is still unclear. A large body of experimental data suggests that
3 increases in the organic fraction of marine aerosol can have implications on hygroscopicity
4 (e.g. Saxena et al., 1995; Fuentes et al., 2011; Ovadenevaite et al., 2013) and could
5 potentially influence our results. Overall, our data analysis shows that an average value of 26
6 sr for clean marine aerosol lidar ratio provides the best agreement between the SODA product
7 and CALIOP retrieved global mean marine aerosol optical depth values. However, our study
8 also shows large spatiotemporal variability in marine aerosol lidar ratios, suggesting that a
9 single constant value of the lidar ratio is not suitable for a wide range of marine aerosol and
10 can lead to large uncertainties at different locations and seasons.

11 We have estimated the error in CALIOP retrieved column integrated attenuated
12 particulate backscatter. Calculations suggest that the average uncertainty in particulate
13 backscatter is more than an order of magnitude lower compared to the retrieved value. Data
14 analysis also showed no clear indication for either approaching a sensitivity limit (due to
15 strong attenuation of the lidar signal throughout the layer) or the contamination of the
16 backscattered signal by the surface reflectance. Based on the conducted error analysis we
17 conclude that the strict quality control criteria developed in this study is adequate to remove
18 the majority of erroneous retrievals.

19 Finally, even though calculations here were carried out for marine aerosol, the
20 technique used in this study is broad and can be used to infer lidar ratios of different species
21 of atmospheric aerosols (i.e., mineral dust, biomass burning, etc.) advecting over the ocean.
22 Because our data analysis shows that it is possible to derive a correction to the CALIOP
23 prescribed marine aerosol lidar ratio, future studies should also consider conducting case
24 studies over different oceanic regions to examine the possible effects of meteorological
25 parameters and ocean physiochemical/biological composition on marine aerosol lidar ratio.
26 Classification (in the form of a look-up table) of spatiotemporal distribution and wind speed
27 dependence of a limited number of parameters mostly affecting marine aerosol lidar ratios,
28 may lead to improved retrievals of AOD values over the oceans.

29

30 **Acknowledgements**

31 This research was supported by the National Aeronautics & Space Administration (NASA)
32 through grant no NNX11AG72G and by the National Science Foundation through the grant
33 AGS-1249273. The authors gratefully acknowledge the CALIPSO, CloudSat, and NASA

1 Langley HSRL Teams for their support and effort in making the data available. CALIPSO
2 data were obtained from the NASA Langley Research Center Atmospheric Science Data
3 Center. CloudSat data are produced by Remote Sensing Systems and sponsored by the NASA
4 Earth Science MEaSURES DISCOVER Project and the Advanced Microwave Scanning
5 Radiometer (AMSR-E) Science Team. The SODA product is developed at the ICARE data
6 and services center (<http://www.icare.univ-lille1.fr>) in Lille (France) in the frame of the
7 CALIPSO mission and supported by CNES.

1 **References**

- 2 Ackermann, J.: The extinction-to-backscatter ratio of tropospheric aerosol: A numerical
3 study, *J. Atmos. Ocean. Technol.*, 15, 1043-1050, doi:
4 10.1175/1520-0426(1998)015<1043:TETBRO>2.0.CO;2, 1998.
- 5 Amiridis, V., Balis, D. S., Giannakaki, E., Stohl, A., Kazadzis, S., Koukouli, M. E. and Zanis,
6 P.: Optical characteristics of biomass burning aerosols over Southeastern Europe
7 determined from UV-Raman lidar measurements, *Atmos. Chem. and Phys.*, 9, 2431-2440,
8 doi:10.5194/acp-9-2431-2009, 2009.
- 9 Andreae, M. O.: Aerosols before Pollution, *Science*, 315, 50-51, 10.2307/20035138, 2007.
- 10 Anguelova, M., Barber Jr, R. P. and Wu, J.: Spume drops produced by the wind tearing of
11 wave crests, *J. Phys. Oceanogr.*, 29, 1156-1165,
12 doi:10.1175/1520-0485(1999)029<1156:CO>2.0.CO;2, 1999.
- 13 Ansmann, A., Riebesell, M. and Weitkamp, C.: Measurement of atmospheric aerosol
14 extinction profiles with a Raman lidar, *Opt. Lett.*, 15, 746-748,
15 doi:10.1364/OL.15.000746, 1990.
- 16 Ansmann, A., Wagner, F., Althausen, D., Müller, D., Herber, A. and Wandinger, U.:
17 European pollution outbreaks during ACE 2: Lofted aerosol plumes observed with Raman
18 lidar at the Portuguese coast, *J. Geophys. Res.*, 106, 20725-20,733,
19 doi:10.1029/2000JD000091, 2001.
- 20 Ansmann, A. and Müller, D.: Lidar and Atmospheric Aerosol Particles, in: Lidar, Weitkamp,
21 C. (Ed.), Springer New York, 105-141, 2005.
- 22 Bentamy, A., Katsaros, K. B., Mestas-Nuñez, A. M., Drennan, W. M., Forde, E. B. and
23 Roquet, H.: Satellite estimates of wind speed and latent heat flux over the global oceans, *J.*
24 *Clim.*, 16, 637-656, doi:10.1175/1520-0442(2003)016<0637:SEOWSA>2.0.CO;2, 2003.
- 25 Blanchard, D. and Woodcock, A.: Bubble formation and modification in the sea and its
26 meteorological significance, *Tellus*, 9, 145-158, doi: 10.1111/j.2153-3490.1957.tb01867.x,
27 1957.
- 28 Bloom, S., Da Silva, A., Dee, D., Bosilovich, M., Chern, J., Pawson, S., Schubert, S.,
29 Sienkiewicz, M., Stajner, I. and Tan, W.: Documentation and validation of the Goddard
30 Earth Observing System (GEOS) data assimilation system–Version 4, NASA Tech.
31 Memo., 104606, 187, 2005.
- 32 Blot, R., Clarke, A. D., Freitag, S., Kapustin, V., Howell, S. G., Jensen, J. B., Shank, L. M.,
33 McNaughton, C. S. and Brekhovskikh, V.: Ultrafine sea spray aerosol over the
34 southeastern Pacific: open-ocean contributions to marine boundary layer CCN, *Atmos.*
35 *Chem. Phys.*, 13, 7263-7278, doi:10.5194/acp-13-7263-2013, 2013.

- 1 Bréon, F. M.: Aerosol extinction-to-backscatter ratio derived from passive satellite
2 measurements, *Atmos. Chem. Phys.*, 13, 8947-8954, doi:10.5194/acp-13-8947-2013,
3 2013.
- 4 Burton, S., Ferrare, R., Hostetler, C., Hair, J., Rogers, R., Obland, M., Butler, C., Cook, A.,
5 Harper, D. and Froyd, K.: Aerosol classification using airborne High Spectral Resolution
6 Lidar measurements—methodology and examples, *Atmos. Meas. Tech.*, 5, 73-98,
7 doi:10.5194/amtd-4-5631-2011, 2012.
- 8 Burton, S. P., Ferrare, R. A., Vaughan, M. A., Omar, A. H., Rogers, R. R., Hostetler, C. A.,
9 and Hair, J. W.: Aerosol classification from airborne HSRL and comparisons with the
10 CALIPSO vertical feature mask, *Atmos. Meas. Tech.*, 6, 1397-1412,
11 doi:10.5194/amt-6-1397-2013, 2013.
- 12 Carslaw, K. S., Lee, L. A., Reddington, C. L., Pringle, K. J., Rap, A., Forster, P. M., Mann,
13 G. W., Spracklen, D. V., Woodhouse, M. T., Regayre, L. A. and Pierce, J. R.: Large
14 contribution of natural aerosols to uncertainty in indirect forcing, *Nature*, 503, 67,
15 doi:10.1038/nature12674.
- 16 Cattrall, C., Reagan, J., Thome, K. and Dubovik, O.: Variability of aerosol and spectral lidar
17 and backscatter and extinction ratios of key aerosol types derived from selected Aerosol
18 Robotic Network locations, *J. Geophys. Res.*, 110, D10S11, doi:10.1029/2004JD005124,
19 2005.
- 20 de Leeuw, G., Andreas, E. L., Anguelova, M. D., Fairall, C., Lewis, E. R., O'Dowd, C.,
21 Schulz, M. and Schwartz, S. E.: Production flux of sea spray aerosol, *Rev. Geophys.*, 49,
22 doi:10.1029/2010RG000349, 2011.
- 23 Doherty, S. J., Anderson, T. L. and Charlson, R. J.: Measurement of the lidar ratio for
24 atmospheric aerosols with a 180 backscatter nephelometer, *Appl. Opt.*, 38, 1823-1832,
25 1999.
- 26 Eloranta, E.: High spectral resolution lidar, in: *Lidar: Range-Resolved Optical Remote
27 Sensing of the Atmosphere*, edited by: Weitkamp, K., Springer, New York, 143-163,
28 2005.
- 29 Fernald, F. G., Herman, B. M. and Reagan, J. A.: Determination of aerosol height
30 distributions by lidar, *J. Appl. Meteorol.*, 11, 482-489, 1972.
- 31 Fuentes, E., Coe, H., Green, D. and McFiggans, G.: On the impacts of phytoplankton-derived
32 organic matter on the properties of the primary marine aerosol - Part 2: Composition,
33 hygroscopicity and cloud condensation activity, *Atmos. Chem. Phys.*, 11, 2585-2602,
34 doi:10.5194/acp-11-2585-2011, 2011.
- 35 Ghan, S., Laulainen, N., Easter, R., Wagener, R., Nemesure, S., Chapman, E., Zhang, Y. and
36 Leung, R.: Evaluation of aerosol direct radiative forcing in MIRAGE, *J. Geophys. Res.*,
37 106, 5295-5316, doi:10.1029/2000JD900502, 2001.

- 1 Groß S., Esselborn, M., Weinzierl, B., Wirth, M., Fix, A. and Petzold, A.: Aerosol
2 classification by airborne high spectral resolution lidar observations, *Atmos. Chem. Phys.*,
3 13, 2487-2505, doi:10.5194/acp-13-2487-2013, 2013.
- 4 Groß, S., Gasteiger, J., Freudenthaler, V., Wiegner, M., Geiß, A., Schladitz, A., Toledano, C.,
5 Kandler, K., Tesche, M., Ansmann, A. and Wiedensohler, A.: Characterization of the
6 planetary boundary layer during SAMUM-2 by means of lidar measurements, *Tellus B*,
7 63, 695-705, doi:10.1111/j.1600-0889.2011.00557.x, 2011a.
- 8 Groß S., Tesche, M., Voker, F., Toledano, C., Wiegner, M., Ansmann, A., Althausen, D.,
9 Seefeldner, M.: Characterization of Saharan dust, marine aerosols and mixtures of
10 biomass-burning aerosols and dust by means of multi-wavelength depolarization and
11 Raman lidar measurements during SAMUM 2, *Tellus B*, 63, 706-724,
12 doi:10.1111/j.1600-0889.2011.00556.x, 2011b.
- 13 Grund, C. J. and Eloranta, E. W.: University of Wisconsin High Spectral Resolution Lidar,
14 *Optical Engineering*, 30, 6-12, doi:10.1117/12.55766, 1991.
- 15 Hair, J. W., Hostetler, C. A., Cook, A. L., Harper, D. B., Ferrare, R. A., Mack, T. L., Welch,
16 W., Izquierdo, L. R. and Hovis, F. E.: Airborne High Spectral Resolution Lidar for
17 profiling aerosol optical properties, *Appl. Opt.*, 47, 6734-6752,
18 doi:10.1364/AO.47.006734, 2008.
- 19 Hoffman, E. J. and Duce, R. A.: The organic carbon content of marine aerosols collected on
20 Bermuda, *J. Geophys. Res.*, 79, 4474-4477, 1974.
- 21 Holben, B. N., Eck, T. F., Slutsker, I., Tanré, D., Buis, J. P., Setzer, A., Vermote, E., Reagan,
22 J. A., Kaufman, Y. J., Nakajima, T., Lavenu, F., Jankowiak, I. and Smirnov, A.:
23 AERONET-A Federated Instrument Network and Data Archive for Aerosol
24 Characterization, *Remote Sens. Environ.*, 66, 1, doi:10.1016/S0034-4257(98)00031-5,
25 1998.
- 26 Hoose, C., Kristjánsson, J., Iversen, T., Kirkevåg, A., Seland, Ø and Gettelman, A.:
27 Constraining cloud droplet number concentration in GCMs suppresses the aerosol indirect
28 effect, *Geophys. Res. Lett.*, 36, L12807, doi:10.1029/2009GL038568, 2009.
- 29 Hostetler, C., Liu, Z., Reagan, J., Vaughan, M., Winker, D., Osborn, M., Hunt, W., Powell,
30 K. and Trepte, C.: CALIOP algorithm theoretical basis document—Part 1: Lidar level I
31 ATBD-Calibration and level 1 data products, *Rep.PC-SCI*, 201, 66, 2005.
- 32 Josset, D., Pelon, J., Protat, A. and Flamant, C.: New approach to determine aerosol optical
33 depth from combined CALIPSO and CloudSat ocean surface echoes, *Geophys. Res. Lett.*,
34 35, L10805, doi:10.1029/2008GL033442, 2008.
- 35 Josset, D., Pelon, J. and Hu, Y.: Multi-instrument calibration method based on a
36 multiwavelength ocean surface model, *Geoscience and Remote Sensing Letters, IEEE*, 7,
37 195-199, doi:10.1109/LGRS.2009.2030906, 2010a.
- 38 Josset, D., Zhai, P., Hu, Y., Pelon, J. and Lucker, P. L.: Lidar equation for ocean surface and
39 subsurface, *Opt. Express*, 18, 20862-20875, doi:10.1364/OE.18.020862, 2010b.

- 1 Josset, D., Rogers, R., Pelon, J., Hu, Y., Liu, Z., Omar, A. and Zhai, P.: CALIPSO lidar ratio
2 retrieval over the ocean, *Opt. Express*, 19, 18696-18706, doi:10.1364/OE.19.018696,
3 2011.
- 4 Josset, D., Pelon, J., Garnier, A., Hu, Y., Vaughan, M., Zhai, P., Kuehn, R. and Lucker, P.:
5 Cirrus optical depth and lidar ratio retrieval from combined CALIPSO-CloudSat
6 observations using ocean surface echo, *J. Geophys. Res.*, 117, D05207,
7 doi:10.1029/2011JD016959, 2012.
- 8 Kaufman, Y. J., Tanré, D. and Boucher, O.: A satellite view of aerosols in the climate system,
9 *Nature*, 419, 215-223, doi:10.1038/nature01091, 2002.
- 10 Kiliyanpilakkil, V. P. and Meskhidze, N.: Deriving the effect of wind speed on clean marine
11 aerosol optical properties using the A-Train satellites, *Atmos. Chem. Phys.*, 11,
12 11401-11413, doi:10.5194/acp-11-11401-2011, 2011.
- 13 Kleidman, R.G., Smirnov, A., Levy, R.C., Mattoo, S., Tanre, D.: Evaluation and Wind Speed
14 Dependence of MODIS Aerosol Retrievals Over Open Ocean, *IEEE T Geosci Remote*,
15 vol.50, no.2, pp.429,435, Feb. 2012, doi:10.1109/TGRS.2011.2162073, 2010.
- 16 Lehahn, Y., Koren, I., Boss, E., Ben-Ami, Y. and Altaratz, O.: Estimating the maritime
17 component of aerosol optical depth and its dependency on surface wind speed using
18 satellite data, *Atmos. Chem. Phys.*, 10, 6711-6720, doi:10.5194/acp-10-6711-2010, 2010.
- 19 Levy, R., Remer, L., Martins, J., Kaufman, Y., Plana-Fattori, A., Redemann, J. and Wenny,
20 B.: Evaluation of the MODIS aerosol retrievals over ocean and land during CLAMS, *J.*
21 *Atmos. Sci.*, 62, 974-992, doi:10.1175/JAS3391.1, 2005.
- 22 Lewis, R. and Schwartz, E.: Sea salt aerosol production: mechanisms, methods,
23 measurements and models—a critical review, American Geophysical Union,
24 doi:10.1029/GM152, 2004.
- 25 Masonis, S. J., Anderson, T. L., Covert, D. S., Kapustin, V., Clarke, A. D., Howell, S. and
26 Moore, K.: A Study of the Extinction-to-Backscatter Ratio of Marine Aerosol during the
27 Shoreline Environment Aerosol Study, *J. Atmos. Ocean. Technol.*, 20, 1388-1402,
28 doi:10.1175/1520-0426(2003)020<1388:ASOTER>2.0.CO;2, 2003.
- 29 Meskhidze, N., Xu, J., Gantt, B., Zhang, Y., Nenes, A., Ghan, S., Liu, X., Easter, R. and
30 Zaveri, R.: Global distribution and climate forcing of marine organic aerosol—Part 1:
31 Model improvements and evaluation, *Atmos. Chem. Phys.*, 11, 11689-11705,
32 doi:10.5194/acp-11-11689-2011, 2011.
- 33 Müller, D., Ansmann, A., Mattis, I., Tesche, M., Wandinger, U., Althausen, D. and Pisani,
34 G.: Aerosol-type-dependent lidar ratios observed with Raman lidar, *J. Geophys. Res.*, 112,
35 10.1029/2006JD008292, 2007.
- 36 Omar, A. H., Winker, D. M., Kittaka, C., Vaughan, M. A., Liu, Z., Hu, Y., Trepte, C. R.,
37 Rogers, R. R., Ferrare, R. A., Lee, K., Kuehn, R. E. and Hostetler, C. A.: The CALIPSO
38 Automated Aerosol Classification and Lidar Ratio Selection Algorithm, *J. Atmos. Ocean.*
39 *Technol.*, 26, 1994-2014, doi:10.1175/2009JTECHA1231.1, 2009.

- 1 Oo, M. and Holz, R.: Improving the CALIOP aerosol optical depth using combined MODIS-
2 CALIOP observations and CALIOP integrated attenuated total color ratio, *J. Geophys.*
3 *Res.*, 116, D14201, doi:10.1029/2010JD014894, 2011.
- 4 Ovadnevaite, J., Ceburnis, D., Martucci, G., Bialek, J., Monahan, C., Rinaldi, M., Facchini,
5 M. C., Berresheim, H., Worsnop, D. R. and O'Dowd, C.: Primary marine organic aerosol:
6 A dichotomy of low hygroscopicity and high CCN activity, *Geophys. Res. Lett.*, 38,
7 doi:10.1029/2011GL048869, 2011.
- 8 Piironen, P. and Eloranta, E.: Demonstration of a high-spectral-resolution lidar based on an
9 iodine absorption filter, *Opt. Lett.*, 19, 234-236, 1994.
- 10 Redemann, J., Vaughan, M. A., Zhang, Q., Shinozuka, Y., Russell, P. B., Livingston, J. M.,
11 Kacenelenbogen, M., and Remer, L. A.: The comparison of MODIS-Aqua (C5) and
12 CALIOP (V2 & V3) aerosol optical depth, *Atmos. Chem. Phys.*, 12, 3025-3043,
13 doi:10.5194/acp-12-3025-2012, 2012.
- 14 Saxena, P., Hildemann, L. M., McMurry, P. H. and Seinfeld, J. H.: Organics alter
15 hygroscopic behavior of atmospheric particles, *J. Geophys. Res.*, 100, 18755-18770,
16 doi:10.1029/95JD01835, 1995.
- 17 Sayer, A., Smirnov, A., Hsu, N. and Holben, B.: A pure marine aerosol model, for use in
18 remote sensing applications, *J. Geophys. Res.*, 117, doi:10.1029/2011JD016689, 2012.
- 19 Schuster, G. L., Vaughan, M., MacDonnell, D., Su, W., Winker, D., Dubovik, O., Lapyonok,
20 T. and Trepte, C.: Comparison of CALIPSO aerosol optical depth retrievals to AERONET
21 measurements, and a climatology for the lidar ratio of dust, *Atmos. Chem. Phys.*, 12,
22 7431-7452, doi:10.5194/acp-12-7431-2012, 2012
- 23 Shipley, S. T., Tracy, D., Eloranta, E. W., Trauger, J. T., Sroga, J., Roesler, F. and Weinman,
24 J. A.: High spectral resolution lidar to measure optical scattering properties of atmospheric
25 aerosols. 1: Theory and instrumentation, *Appl. Opt.*, 22, 3716-3724, 1983.
- 26 Smirnov, A., Holben, B., Eck, T., Dubovik, O. and Slutsker, I.: Effect of wind speed on
27 columnar aerosol optical properties at Midway Island, *J. Geophys. Res.*, 108(D24), 4802,
28 doi:10.1029/2003JD003879, 2003.
- 29 Smirnov, A., Holben, B. N., Giles, D. M., Slutsker, I., O'Neill, N. T., Eck, T. F., Macke, A.,
30 Croot, P., Courcoux, Y., Sakerin, S. M., Smyth, T. J., Zielinski, T., Zibordi, G., Goes, J. I.,
31 Harvey, M. J., Quinn, P. K., Nelson, N. B., Radionov, V. F., Duarte, C. M., Losno, R.,
32 Sciare, J., Voss, K. J., Kinne, S., Nalli, N. R., Joseph, E., Krishna Moorthy, K.,
33 Covert, D. S., Gulev, S. K., Milinevsky, G., Larouche, P., Belanger, S., Horne, E.,
34 Chin, M., Remer, L. A., Kahn, R. A., Reid, J. S., Schulz, M., Heald, C. L., Zhang, J.,
35 Lapina, K., Kleidman, R. G., Griesfeller, J., Gaitley, B. J., Tan, Q., and Diehl, T. L.:
36 Maritime aerosol network as a component of AERONET – first results and comparison
37 with global aerosol models and satellite retrievals, *Atmos. Meas. Tech.*, 4, 583-597,
38 doi:10.5194/amt-4-583-2011, 2011.
- 39 Smirnov, A., Holben, B. N., Slutsker, I., Giles, D. M., McClain, C. R., Eck, T. F., Sakerin, S.
40 M., Macke, A., Croot, P., Zibordi, G., Quinn P. K., Sciare, J., Kinne, S., Harvey, M.,

- 1 Smyth, T. J., Piketh S., Zielinski, T., Proshutinsky A., Goes, J. I., Nelson, N. B., Larouche,
2 P., Radionov, V. F., Goloub, P., Krishna Moorthy, K., Matarrese, R., Robertson, E. J. and
3 Jourdin, F.: Maritime Aerosol Network as a component of Aerosol Robotic Network, *J.*
4 *Geophys. Res.*, 114, D06204, doi:10.1029/2008JD011257, 2009.
- 5 Tesche, M., Ansmann, A., Müller, D., Althausen, D., Engelmann, R., Freudenthaler, V. and
6 Groß, S.: Vertically resolved separation of dust and smoke over Cape Verde using
7 multiwavelength Raman and polarization lidars during Saharan Mineral Dust Experiment
8 2008, *J. Geophys. Res.*, 114, n/a-n/a, doi:10.1029/2009JD011862, 2009a.
- 9 Tesche, M., Ansmann, A., Müller, D., Althausen, D., Mattis, I., Heese, B., Freudenthaler, V.,
10 Wiegner, M., Esselborn, M., Pisani, G., and Knippertz, P.: Vertical profiling of Saharan
11 dust with Raman lidars and airborne HSRL in southern Morocco during SAMUM, *Tellus*
12 *B*, 61, 144-164, doi:10.1111/j.1600-0889.2008.00390.x, 2009b.
- 13 Vaughan, M. A., Young, S. A., Winker, D. M., Powell, K. A., Omar, A. H., Liu, Z., Hu, Y.
14 and Hostetler, C. A.: Fully automated analysis of space-based lidar data: An overview of
15 the CALIPSO retrieval algorithms and data products, *Proc. SPIE 5575, Laser Radar*
16 *Techniques for Atmospheric Sensing*, 16, doi:10.1117/12.572024, 2004.
- 17 Vaughan, M. A., Powell, K. A., Kuehn, R. E., Young, S. A., Winker, D. M., Hostetler, C. A.,
18 Hunt, W. H., Liu Z., McGill, M. J. and Getzewich, B. J.: Fully automated detection of
19 cloud and aerosol layers in the CALIPSO lidar measurements, *J. Atmos. Ocean Technol.*,
20 26, 2034-2050, doi:10.1175/2009JTECHA1228.1, 2009.
- 21 Wang, M. and Penner, J.: Aerosol indirect forcing in a global model with particle nucleation,
22 *Atmos. Chem. Phys.*, 9, 239-260, doi:10.5194/acp-9-239-2009, 2009.
- 23 Westervelt, D., Moore, R., Nenes, A. and Adams, P.: Effect of primary organic sea spray
24 emissions on cloud condensation nuclei concentrations, *Atmos. Chem. Phys.*, 12, 89-101,
25 doi:10.5194/acp-12-89-2012, 2012.
- 26 Winker, D. M., Vaughan, M. A., Omar, A., Hu, Y., Powell, K. A., Liu, Z., Hunt, W. H. and
27 Young, S. A.: Overview of the CALIPSO mission and CALIOP data processing
28 algorithms, *J. Atmos. Ocean. Technol.*, 26, 2310-2323, doi:10.1175/2009JTECHA1281.1
29 2009.
- 30 Young, S. A., Cutten, D. R., Lynch, M. J. and Davies, J. E.: Lidar-derived variations in the
31 backscatter-to-extinction ratio in southern hemisphere coastal maritime aerosols, *Atmos.*
32 *Environ.*, 27, 1541-1551, doi:10.1016/0960-1686(93)90154-Q, 1993.
- 33 Young, S. A. and Vaughan, M. A.: The retrieval of profiles of particulate extinction from
34 cloud-aerosol lidar infrared pathfinder satellite observations (CALIPSO) data: algorithm
35 description, *J. Atmos. Oceanic Technol.*, 26, 1105-1119,
36 doi:10.1175/2008JTECHA1221.1, 2009.

37

38

1 **Tables**

2

3 **Table 1.** Seasonal means \pm 1 standard deviations for $2^\circ \times 5^\circ$ grid cell medians. The
4 subscripts p, S, and C appended to τ stand for particulate, SODA, and CALIOP,
5 respectively, where τ is the AOD.
6
7

Season	SODA $\tau_{p,S}$	CALIOP $\tau_{p,C}$	$\Gamma_p, \times 10^{-3}$ sr ⁻¹	S_p sr
Winter	0.14 \pm 0.04	0.09 \pm 0.03	4.7 \pm 1.2	27 \pm 8
Spring	0.13 \pm 0.03	0.09 \pm 0.03	4.8 \pm 1.2	24 \pm 7
Summer	0.14 \pm 0.04	0.09 \pm 0.03	4.6 \pm 1.2	27 \pm 8
Fall	0.13 \pm 0.03	0.09 \pm 0.03	4.7 \pm 1.1	25 \pm 7

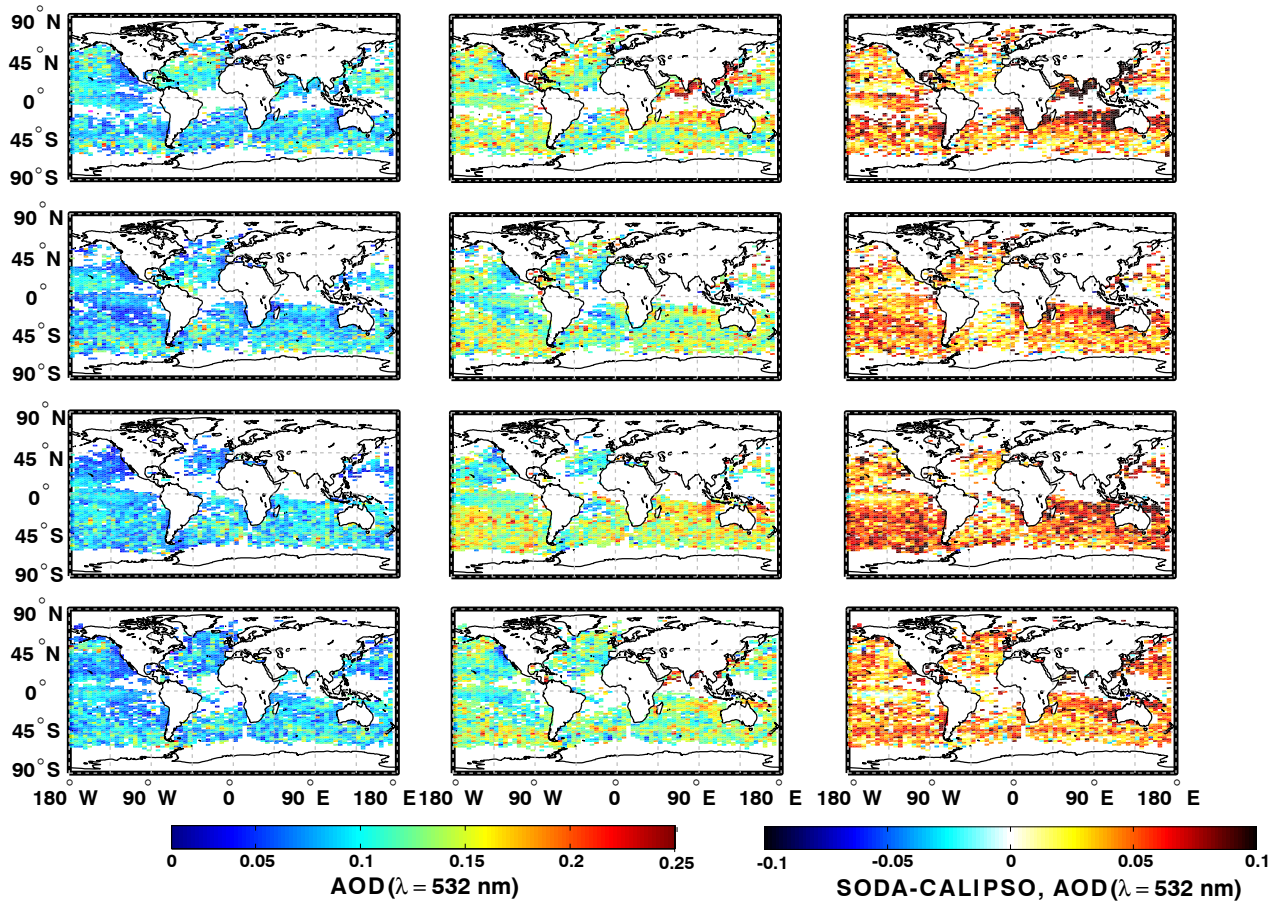
8

9

1 **Table 2.** Means \pm 1 standard deviation for $2^\circ \times 5^\circ$ grid cell medians for various AMSR-E
 2 wind speed regimes. The subscripts S and C appended to τ stand for SODA and CALIOP,
 3 respectively, where τ is the AOD.
 4

Wind Regime ms^{-1}	SODA τ_S	CALIOP τ_C	$\Gamma_p, \times 10^{-3}$ sr^{-1}	S_p sr	Number absolute(%)
$0 < U_{10} \leq 4$	0.12 \pm 0.05	0.07 \pm 0.04	3.6 \pm 1.4	32 \pm 17	11849 (5)
$4 < U_{10} \leq 6$	0.11 \pm 0.04	0.07 \pm 0.03	3.8 \pm 1.1	27 \pm 12	32899 (13)
$6 < U_{10} \leq 8$	0.12 \pm 0.04	0.08 \pm 0.02	4.2 \pm 1.0	26 \pm 9	60083 (23)
$8 < U_{10} \leq 10$	0.13 \pm 0.03	0.08 \pm 0.02	4.7 \pm 1.0	26 \pm 7	68899 (26)
$10 < U_{10} \leq 12$	0.15 \pm 0.04	0.10 \pm 0.03	5.1 \pm 1.0	26 \pm 6	45895 (17)
$12 < U_{10} \leq 15$	0.16 \pm 0.04	0.12 \pm 0.03	5.7 \pm 1.2	25 \pm 6	30162 (11)
$U_{10} > 15$	0.16 \pm 0.04	0.14 \pm 0.04	6.4 \pm 1.4	22 \pm 7	12953 (5)

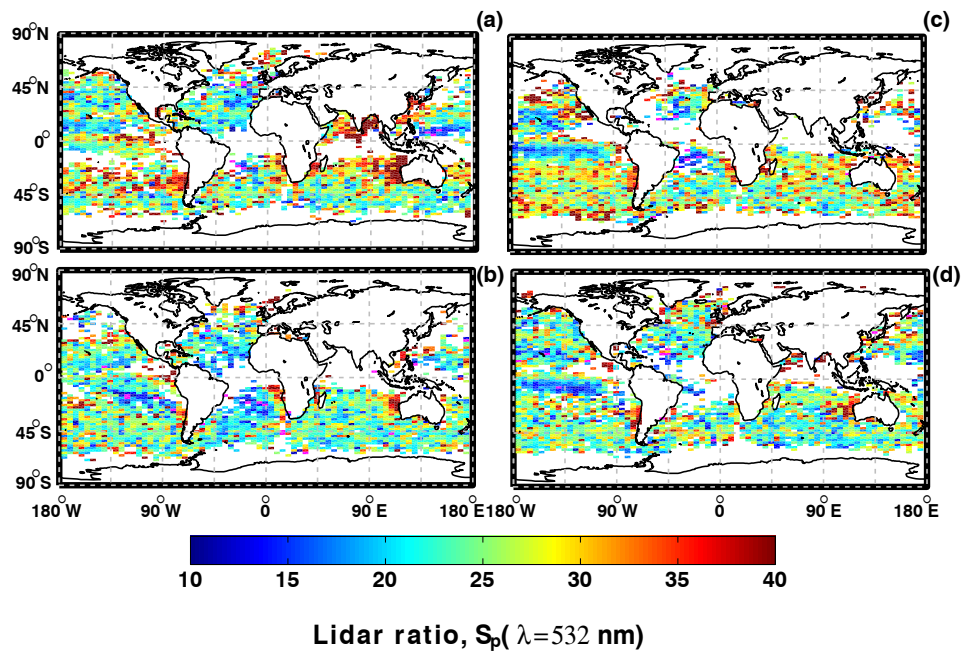
1 Figures



2

3 **Fig. 1** - Seasonal median AOD values from CALIOP and SODA (columns 1 and 2) and the
 4 difference (SODA – CALIOP) plot (column 3) for December - February (row 1), March -
 5 May (row 2), June - August (row 3), September - November (row 4) plotted on a $2^\circ \times 5^\circ$
 6 latitude longitude grid. “No Data” is shaded white and is defined as grid cells failing quality
 7 control algorithm (see text for details).

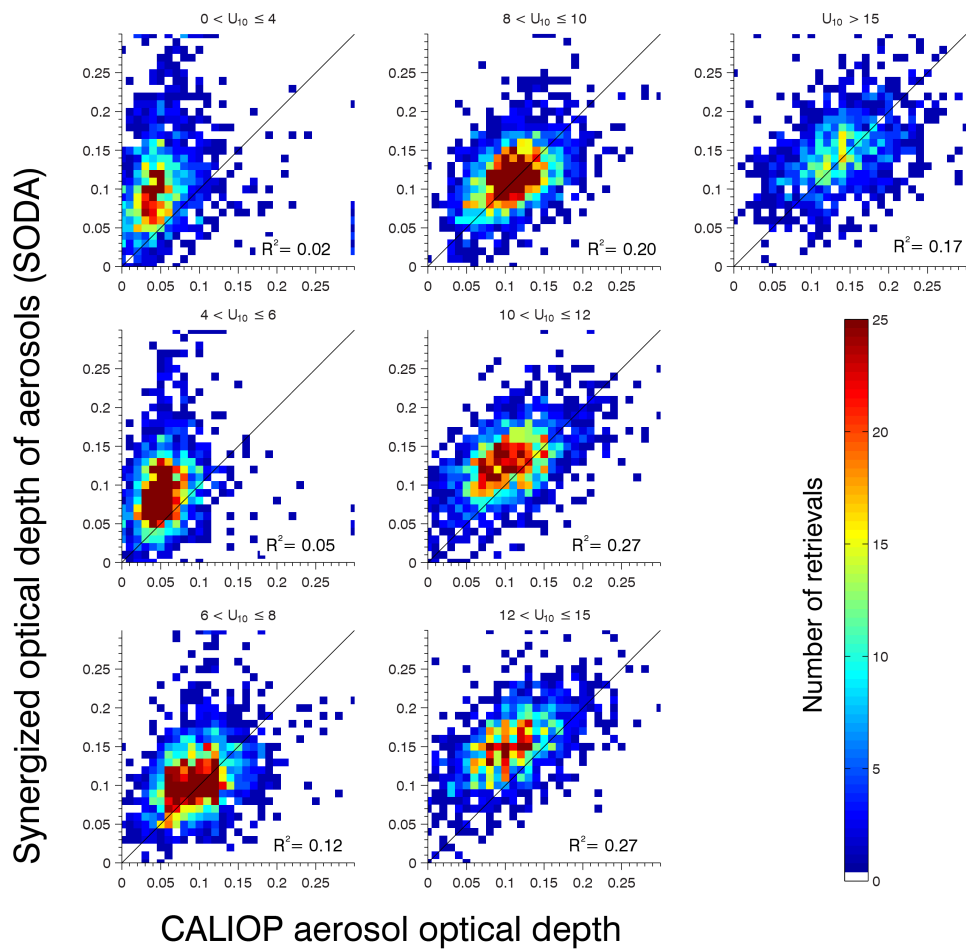
8



1

2 **Fig. 2** - Seasonal lidar ratio for $2^\circ \times 5^\circ$ latitude longitude grid cells. Seasons are arranged as
 3 (a) December - February , (b) March - May, (c) June - August, (d) September - November.

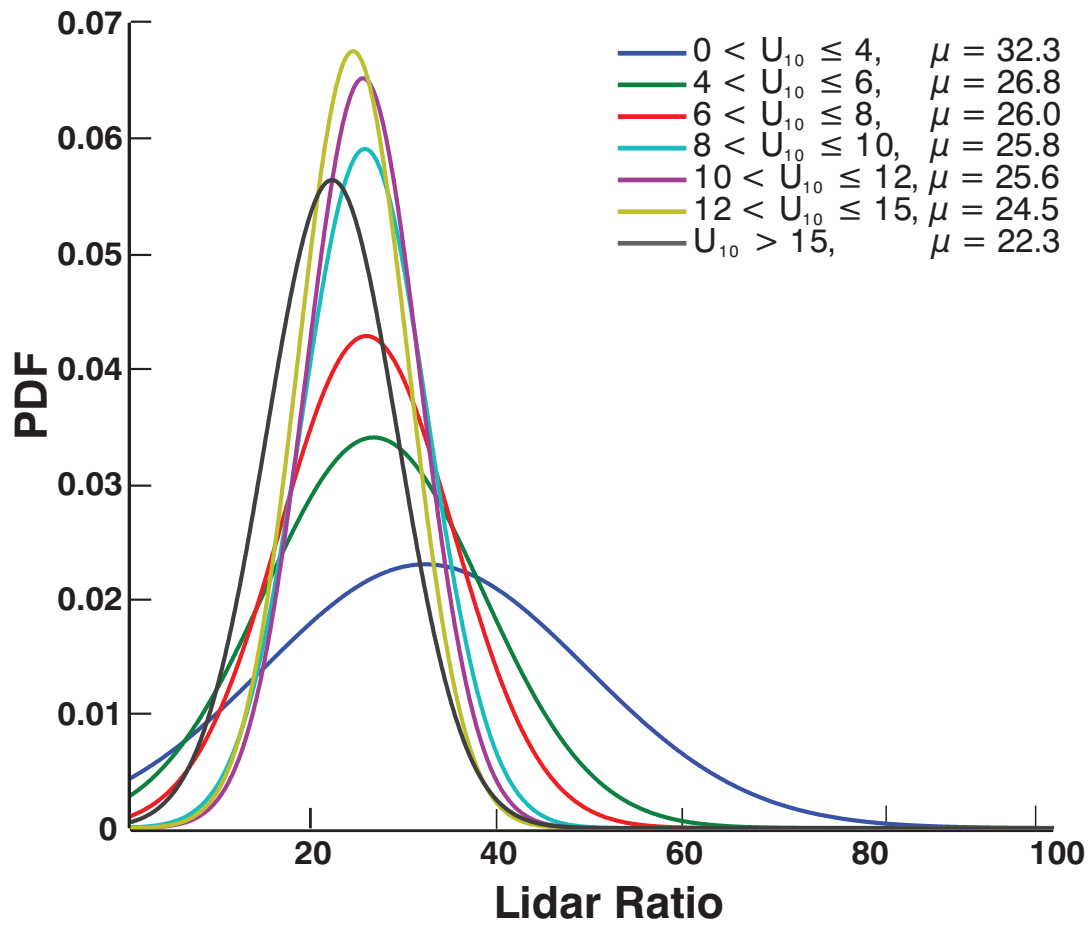
4



1

2 **Fig. 3** - Scatter density plot of SODA to CALIOP AOD for each wind speed regime. Each
 3 point indicates a grid cell median, colored by frequency of occurrence. The black line is the
 4 1:1 relationship, with reported R^2 values.

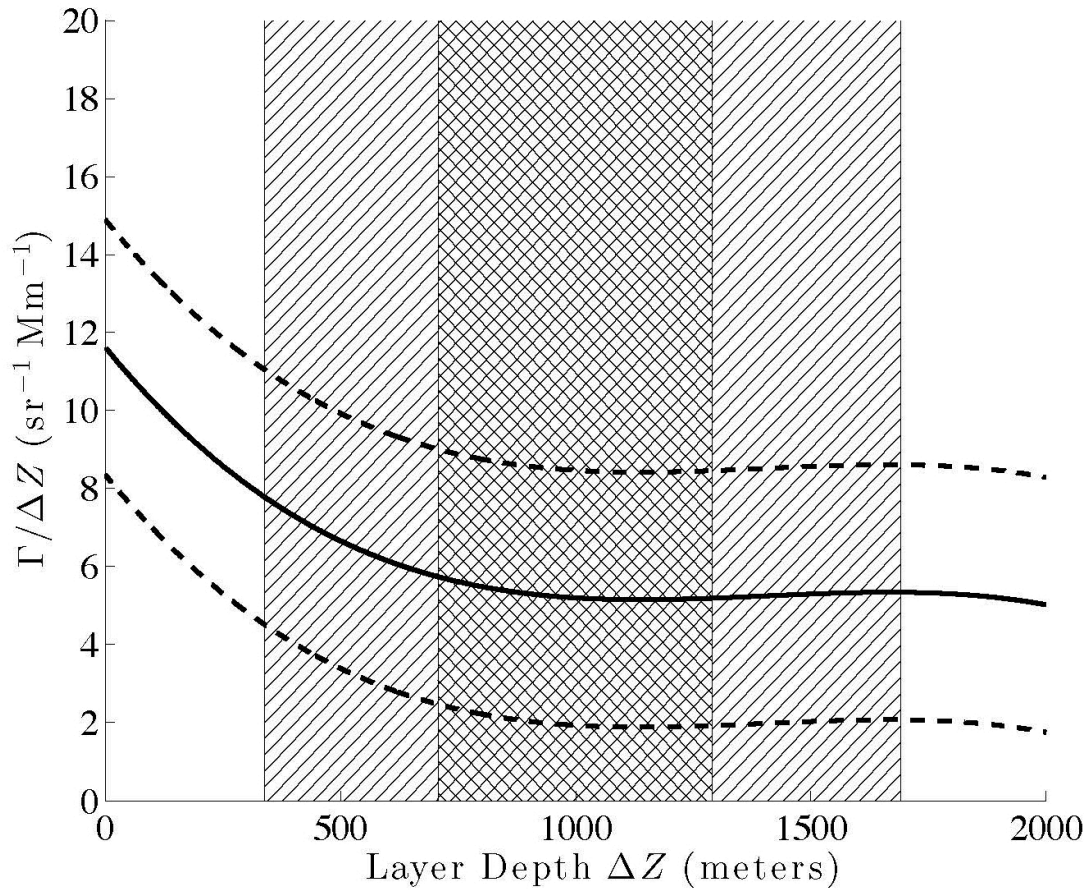
5



1

2 **Fig. 4** - Probability density function of clean marine aerosol lidar ratio for selected AMSR-E
 3 wind speed regimes. The mean (μ) of each distribution is also reported.

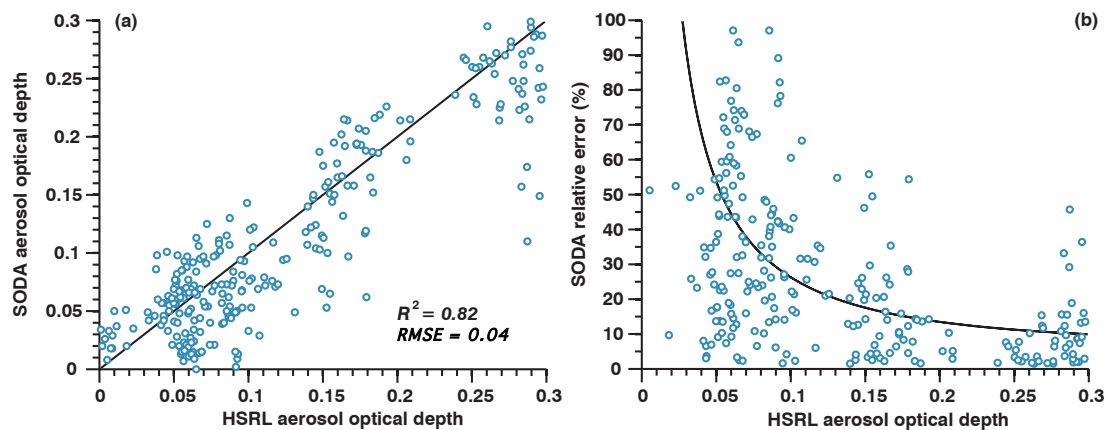
4



1

2 **Fig. 5** - The normalised integrated attenuated backscatter as a function of the layer depth. The
 3 solid line shows the 3rd order least squares fit to the data while the dotted lines show $\pm 1\sigma$; the
 4 hatched area shows the layer depth data frequency: cross hatch between the 25th and 75th
 5 percentiles and straight hatch between 5th and 95th percentiles.

6



1
2
3
4
5
6
7
8

Fig. 6 (a) A scatter plot of SODA AOD relative to AOD measured by HSRL at 532 nm with corresponding R^2 and RMSE. The black line illustrates the 1:1 line. (b) Relative uncertainty in the SODA column lidar ratio as a function of HSRL AOD with the black line showing the least squares exponential fit as in Josset et al. (2012), Eq. 15. All points are classified as marine plus pollution or marine plus dust and are from Table 1 in Josset et al. (2011).

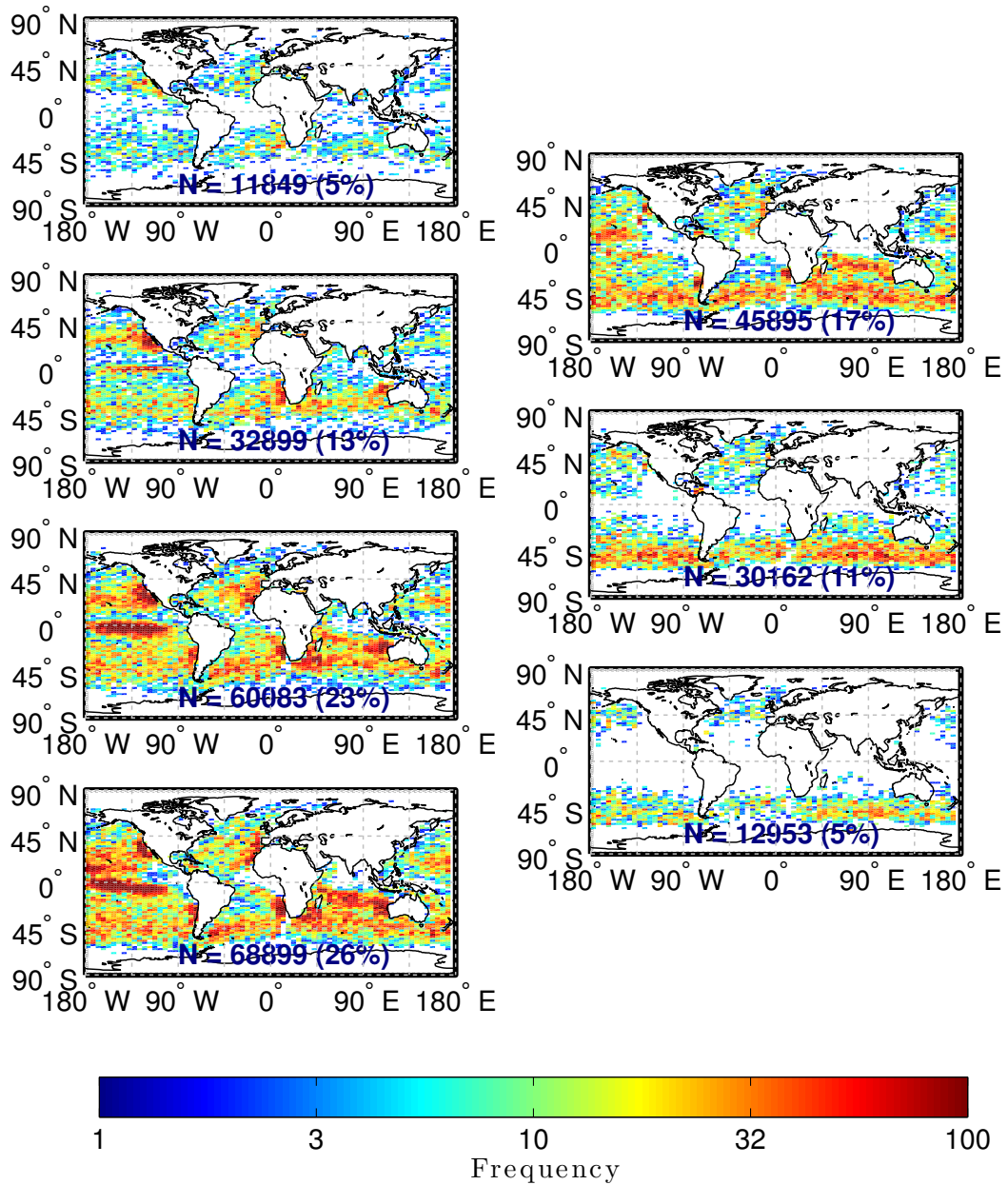
Supplementary Information

Table S1. Common techniques for measuring the lidar ratio along with some values reported for marine aerosol at, or near, 532 nm wavelength.

Instrumentation	Type	Operating Principle	$S_{p,532}$ (sr)
Raman Lidar ^(b)	Direct	Light is scattered at a different wavelength than the incident laser. Aerosol extinction is calculated by the Raman lidar equation. Rayleigh coefficients for molecular attenuation are calculated with measured or modeled temperature and pressure profiles. The ratio of inelastic (shifted wavelength due to aerosol scattering) backscatter to the elastic (same wavelength) backscatter determines the aerosol backscatter. The particulate lidar ratio is then the aerosol extinction-to-backscatter.	$23 \pm 3^{(a)}$
			$23 \pm 5^{(a)}$
			$18 \pm 2^{(c,d)}$
HSRL Lidar ^(h)	Direct	The HSRL technique relies on the difference in spectral distribution of backscattered signal from molecules and particulates. Discrimination between aerosol/cloud and molecular returns in the receiver is accomplished by splitting the returned signal into two optical channels: the molecular backscatter channel, which is equipped with an extremely narrowband iodine vapor absorption filter to eliminate the aerosol returns and pass the wings of the molecular spectrum, and the total backscatter channel, which passes all frequencies of the returned signal. After appropriate internal calibration of the sensitivities of the two channels, the signals are used to derive profiles of extinction, backscatter coefficient, and extinction-to-backscatter ratio, S_p .	$18 \pm 5^{(e)}$
			$15 - 25^{(f)}$
			$17 - 27^{(g)}$
Modeled with measured size distributions ⁽ⁱ⁾	Indirect	The aerosol size distribution is measured and used with Mie theory (with an assigned or measured refractive index) to retrieve aerosol extinction and backscatter and thereby the lidar ratio. AERONET (Holben et al., 1998) uses an inversion procedure from radiance data collected by sun photometers to derive the aerosol size distribution.	$28^{*(i)}$ $25.4 \pm 3.5^{(j)}$ $29^{\$(k)}$
Phase function and single scattering albedo measurements ^(l)	Indirect	The lidar ratio is also written as the inverse of the single scattering albedo and phase function at 180° . Passive instruments like the POLARization and Directionality of the Earth's Reflectances (POLDER) radiometer retrieve aerosol scattering at multiple angles to determine the phase function and retrieve the lidar ratio. This can also be done with lidar and backscattering nephelometers.	$25^{(l)}$ $21.3 \pm 3.7^{\$(m)}$

(a) Müller et al. (2007); (b) Ansmann and Müller (2005); (c,d,e) Groß et al. (2011a; 2011b; 2013); (f,g) Burton et al. (2012; 2013); (h) Hair et al. (2008); (i) Sayer et al. (2012); (j) Masonis et al. (2003); (k) Cattrall et al. (2005); (l) Bréon (2013); (m) Doherty et al. (1999). * signifies a suggested value, § signifies 550 nm and § refers to a nephelometer study where extinction and backscatter were separately measured.

(b) Direct retrievals are those that measure aerosol extinction and backscatter explicitly. Indirect retrievals are those that rely on inversion algorithms, size distribution assumptions (fine/coarse mode partitioning), chemical composition assumptions (i.e. refractive index), etc. to back out the lidar ratio from retrieval results (this study is an indirect method for determining the lidar ratio).

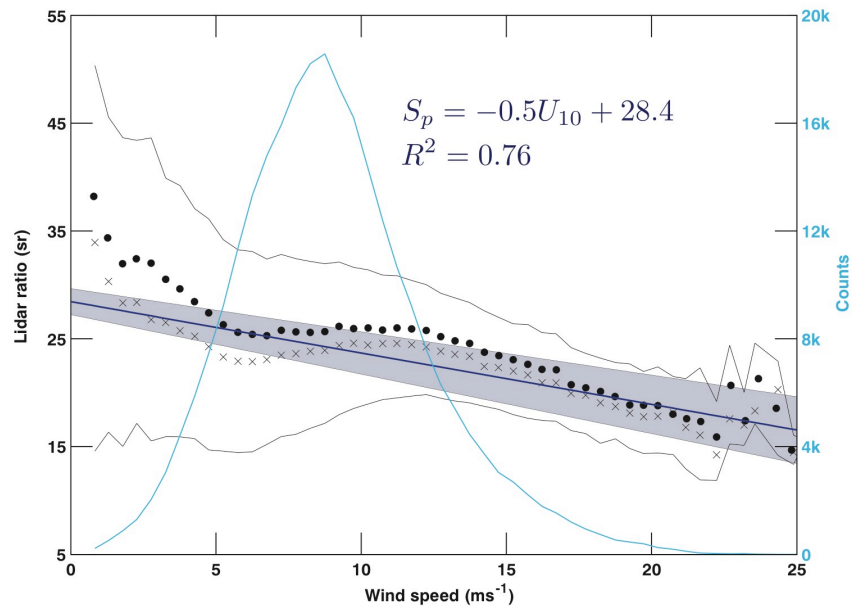


1
2

3 **Fig S1.** CALIOP retrieval counts for each 2° × 5° latitude longitude grid cell and different
 4 wind speed regimes. Total number and percent of total (in parenthesis) is also reported for
 5 each wind regime. Wind speed regimes for column 1 from top to bottom, are 0-4, 4-6, 6-8,
 6 and 8-10 m s⁻¹ and column 2 from top to bottom are 10-12, 12-15, and >15 m s⁻¹.

7

1



2

3

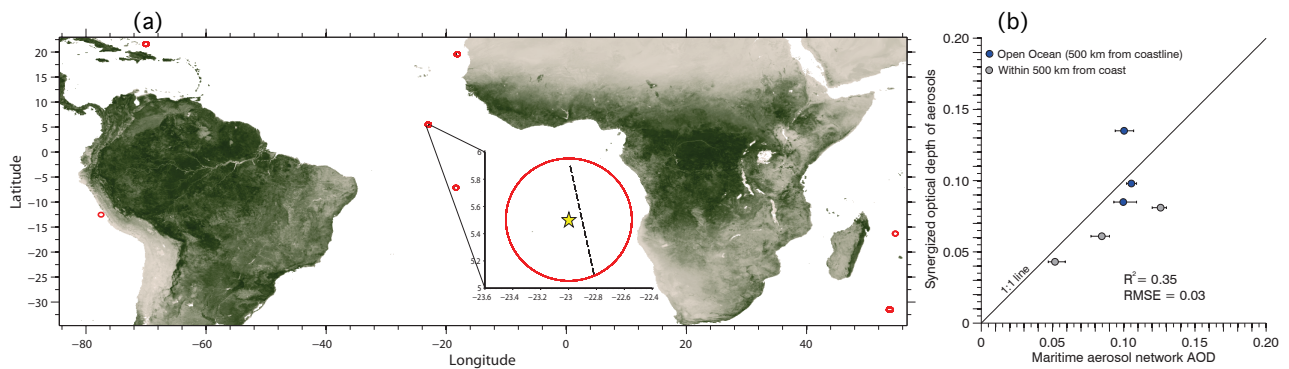
4 **Fig S2.** Median lidar ratio as a function of wind speed (dark blue line). The solid black lines
5 correspond to the 25th (lower) and 75th (upper) percentiles for each data point. Black crosses
6 (dots) are median (mean) lidar ratios for each wind speed bin at 0.5 ms⁻¹ intervals. The light
7 blue line corresponds to the number of retrievals shown on the y-axis to the right. The
8 equation for the least squares linear regression is $S_p = -0.5U_{10} + 28.4$ with an
9 $R^2 = 0.76$. The shaded region is the 95% confidence interval of the fit.

10

1 SODA/MAN Comparison

2
3 Here we have retrieved daytime SODA data for the same time period (years 2007-2010) in
4 order to compare it with the Maritime Aerosol Network (MAN; Smirnov et al., 2009)
5 observations of aerosol optical depth. The MAN observations are made with handheld
6 sunphotometers on ships and report the AOD at a number of wavelengths. In order to most
7 accurately reference the MAN observations to the SODA retrievals of AOD, we corrected
8 MAN AOD at 500 nm to 532 nm by the 500/675 nm angstrom exponent. Then we employed
9 the collocation scheme from Smirnov et al. (2011) and Kleidman et al. (2010). In brief, the
10 collocation scheme required the closest SODA overpass within ± 30 minutes of the MAN
11 measurement and no more than 25 km in radius from the ship. The results are presented
12 below in supplementary Fig. S3. There were 51 matches in total in 6 locations for the selected
13 measurement period. Some points shown in (a) of Fig. S3 are not presented in (b) since there
14 were too few MAN measurements ($N < 2$) to assess the range of AOD.

15
16 The results of the comparison reveal that MAN and SODA compare reasonably well. There
17 appears to surface a negative bias of SODA compared to MAN for reasons unknown. These
18 results are also required to pass the SODA feature classification flag of pure aerosol and no
19 thin cloud. There are, however, no other requirements in the feature classification as data
20 points would become even more sparse making this comparison infeasible.



21
22 **Fig S3.** Map of collocated instances for SODA and MAN measurements of aerosol optical
23 depth (a). Red circles indicate the region where a satellite track resides and the inset displays
24 the satellite track (dashed line) in comparison to the MAN measurement (yellow star). Scatter
25 plot comparing closest SODA to mean MAN aerosol optical depth (b). The error bars
26 indicate the range of MAN reported AOD within a ± 30 minute SODA overpass. The R^2 and
27 RMSE are also shown. Blue circles indicate points at least 500 km from the nearest coastline.

SODA CALIPSO comparison of aerosol optical depth

These plots show the distribution of errors between SODA and CALIOP aerosol optical depth retrievals. We show scatter density plots in Fig. S4 (a) along with the distribution of errors in Fig. S4 (b-c). These plots compare the grid cell medians for all of the data used in the manuscript and total 13,481 points. The distribution of errors show that the RMS error is 0.06. Redemann et al. (2012) stated that for RMS error < 0.1 , the combination of instruments can be used to obtain further information on aerosol optical properties. The distribution of errors is evaluated to obtain the median error of 47%. The CALIOP retrieved AOD is directly a function of the prescribed lidar ratio and is a major contributor to the bias shown in Fig. S4 (a). An increase in the prescribed lidar ratio would mitigate some of this bias.

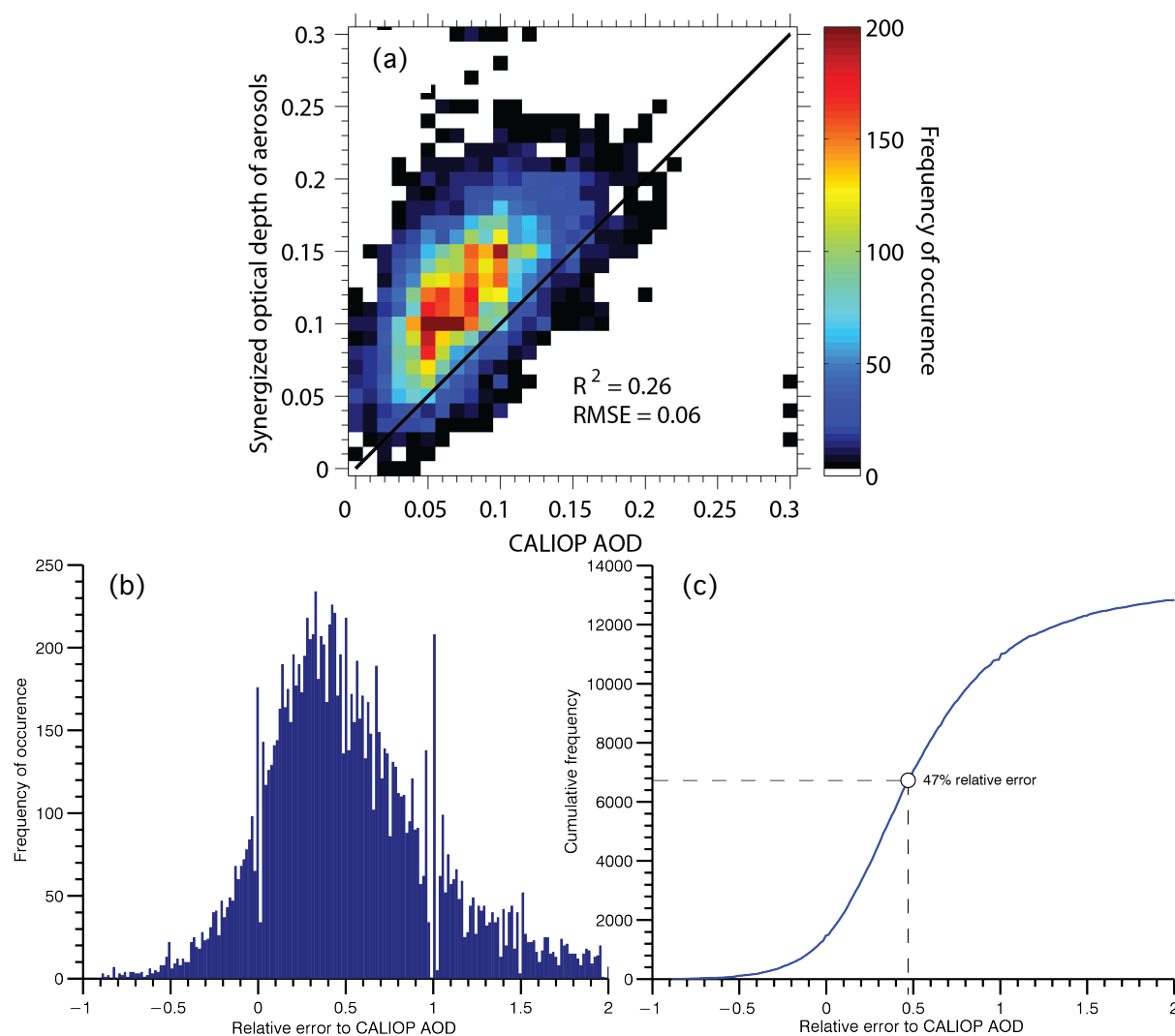


Fig. S4. (a) Scatter density plot of all available (13,481 occurrences) SODA to CALIOP aerosol optical depth data. Each point indicates a grid cell median from the spatial maps shown in the main manuscript. The solid black line is the 1:1 relation. The R^2 value is 0.26 and the RMS error is 0.06. (b) Histogram of the relative error of SODA compared to CALIOP for each of the points indicated in (a). (c) Cumulative error with the median value reported at 47%.

1 References

- 2 Ansmann, A. and Müller, D.: Lidar and Atmospheric Aerosol Particles, in: Lidar, Weitkamp,
3 C. (Ed.), Springer New York, 105-141, 2005.
- 4 Bréon, F. M.: Aerosol extinction-to-backscatter ratio derived from passive satellite
5 measurements, *Atmos. Chem. Phys.*, 13, 8947-8954, doi:10.5194/acp-13-8947-2013,
6 2013.
- 7 Burton, S. P., Ferrare, R. A., Vaughan, M. A., Omar, A. H., Rogers, R. R., Hostetler, C. A.,
8 and Hair, J. W.: Aerosol classification from airborne HSRL and comparisons with the
9 CALIPSO vertical feature mask, *Atmos. Meas. Tech.*, 6, 1397-1412,
10 doi:10.5194/amt-6-1397-2013, 2013.
- 11 Burton, S., Ferrare, R., Hostetler, C., Hair, J., Rogers, R., Obland, M., Butler, C., Cook, A.,
12 Harper, D. and Froyd, K.: Aerosol classification using airborne High Spectral Resolution
13 Lidar measurements—methodology and examples, *Atmos. Meas. Tech.*, 5, 73-98,
14 doi:10.5194/amtd-4-5631-2011, 2012.
- 15 Catrall, C., Reagan, J., Thome, K. and Dubovik, O.: Variability of aerosol and spectral lidar
16 and backscatter and extinction ratios of key aerosol types derived from selected Aerosol
17 Robotic Network locations, *J. Geophys. Res.*, 110, D10S11, doi:10.1029/2004JD005124,
18 2005.
- 19 Doherty, S. J., Anderson, T. L. and Charlson, R. J.: Measurement of the lidar ratio for
20 atmospheric aerosols with a 180 backscatter nephelometer, *Appl. Opt.*, 38, 1823-1832,
21 1999.
- 22 Groß S., Esselborn, M., Weinzierl, B., Wirth, M., Fix, A. and Petzold, A.: Aerosol
23 classification by airborne high spectral resolution lidar observations, *Atmos. Chem. Phys.*,
24 13, 2487-2505, doi:10.5194/acp-13-2487-2013, 2013.
- 25 Groß S., Tesche, M., Voker, F., Toledano, C., Wiegner, M., Ansmann, A., Althausen, D.,
26 Seefeldner, M.: Characterization of Saharan dust, marine aerosols and mixtures of
27 biomass-burning aerosols and dust by means of multi-wavelength depolarization and
28 Raman lidar measurements during SAMUM 2, *Tellus B*, 63, 706-724,
29 doi:10.1111/j.1600-0889.2011.00556.x, 2011b.
- 30 Groß, S., Gasteiger, J., Freudenthaler, V., Wiegner, M., Geiß, A., Schladitz, A., Toledano, C.,
31 Kandler, K., Tesche, M., Ansmann, A. and Wiedensohler, A.: Characterization of the
32 planetary boundary layer during SAMUM-2 by means of lidar measurements, *Tellus B*,
33 63, 695-705, doi:10.1111/j.1600-0889.2011.00557.x, 2011a.
- 34 Hair, J. W., Hostetler, C. A., Cook, A. L., Harper, D. B., Ferrare, R. A., Mack, T. L., Welch,
35 W., Izquierdo, L. R. and Hovis, F. E.: Airborne High Spectral Resolution Lidar for
36 profiling aerosol optical properties, *Appl. Opt.*, 47, 6734-6752,
37 doi:10.1364/AO.47.006734, 2008.
- 38 Kleidman, R.G., Smirnov, A., Levy, R.C., Mattoo, S., Tanre, D.: Evaluation and Wind Speed
39 Dependence of MODIS Aerosol Retrievals Over Open Ocean, *IEEE T Geosci Remote*,

- 1 vol.50, no.2, pp.429,435, Feb. 2012, doi:10.1109/TGRS.2011.2162073, 2010.
- 2 Masonis, S. J., Anderson, T. L., Covert, D. S., Kapustin, V., Clarke, A. D., Howell, S. and
3 Moore, K.: A Study of the Extinction-to-Backscatter Ratio of Marine Aerosol during the
4 Shoreline Environment Aerosol Study, *J. Atmos. Ocean. Technol.*, 20, 1388-1402,
5 doi:10.1175/1520-0426(2003)020<1388:ASOTER>2.0.CO;2, 2003.
- 6 Müller, D., Ansmann, A., Mattis, I., Tesche, M., Wandinger, U., Althausen, D. and Pisani,
7 G.: Aerosol-type-dependent lidar ratios observed with Raman lidar, *J. Geophys. Res.*, 112,
8 10.1029/2006JD008292, 2007.
- 9 Redemann, J., Vaughan, M. A., Zhang, Q., Shinozuka, Y., Russell, P. B., Livingston, J. M.,
10 Kacenenbogen, M., and Remer, L. A.: The comparison of MODIS-Aqua (C5) and
11 CALIOP (V2 & V3) aerosol optical depth, *Atmos. Chem. Phys.*, 12, 3025-3043,
12 doi:10.5194/acp-12-3025-2012, 2012.
- 13 Sayer, A., Smirnov, A., Hsu, N. and Holben, B.: A pure marine aerosol model, for use in
14 remote sensing applications, *J. Geophys. Res.*, 117, doi:10.1029/2011JD016689, 2012.
- 15 Smirnov, A., Holben, B. N., Giles, D. M., Slutsker, I., O'Neill, N. T., Eck, T. F., Macke, A.,
16 Croot, P., Courcoux, Y., Sakerin, S. M., Smyth, T. J., Zielinski, T., Zibordi, G., Goes, J. I.,
17 Harvey, M. J., Quinn, P. K., Nelson, N. B., Radionov, V. F., Duarte, C. M., Losno, R.,
18 Sciare, J., Voss, K. J., Kinne, S., Nalli, N. R., Joseph, E., Krishna Moorthy, K.,
19 Covert, D. S., Gulev, S. K., Milinevsky, G., Larouche, P., Belanger, S., Horne, E.,
20 Chin, M., Remer, L. A., Kahn, R. A., Reid, J. S., Schulz, M., Heald, C. L., Zhang, J.,
21 Lapina, K., Kleidman, R. G., Griesfeller, J., Gaitley, B. J., Tan, Q., and Diehl, T. L.:
22 Maritime aerosol network as a component of AERONET – first results and comparison
23 with global aerosol models and satellite retrievals, *Atmos. Meas. Tech.*, 4, 583-597,
24 doi:10.5194/amt-4-583-2011, 2011.
- 25 Smirnov, A., Holben, B. N., Slutsker, I., Giles, D. M., McClain, C. R., Eck, T. F., Sakerin, S.
26 M., Macke, A., Croot, P., Zibordi, G., Quinn P. K., Sciare, J., Kinne, S., Harvey, M.,
27 Smyth, T. J., Piketh S., Zielinski, T., Proshutinsky A., Goes, J. I., Nelson, N. B., Larouche,
28 P., Radionov, V. F., Goloub, P., Krishna Moorthy, K., Matarrese, R., Robertson, E. J. and
29 Jourdin, F.: Maritime Aerosol Network as a component of Aerosol Robotic Network, *J.*
30 *Geophys. Res.*, 114, D06204, doi:10.1029/2008JD011257, 2009.